



On the relationship between ecosystem-scale hyperspectral reflectance and CO₂ exchange in European mountain grasslands

M. Balzarolo¹, L. Vescovo^{2,3}, A. Hammerle⁴, D. Gianelle^{2,3}, D. Papale⁵, E. Tomelleri⁶, and G. Wohlfahrt^{4,6}

¹Centre of Excellence PLECO, University of Antwerpen, Wilrijk, Belgium

²Forests and Biogeochemical Cycles Research Group, Sustainable Agro-Ecosystems and Bioresources Department, Research and Innovation Centre – Fondazione Edmund Mach, S. Michele all'Adige (TN), Italy

³FoxLaB Research and Innovation Centre – Fondazione Edmund Mach, S. Michele all'Adige (TN), Italy

⁴Institute of Ecology, University of Innsbruck, Innsbruck, Austria

⁵DIBAF, University of Tuscia, Viterbo, Italy

⁶European Academy of Bolzano, Bolzano, Italy

Correspondence to: M. Balzarolo (manuela.balzarolo@uantwerpen.be)

Received: 11 June 2014 – Published in Biogeosciences Discuss.: 1 July 2014

Revised: 21 April 2015 – Accepted: 28 April 2015 – Published: 28 May 2015

Abstract. In this paper we explore the skill of hyperspectral reflectance measurements and vegetation indices (VIs) derived from these in estimating carbon dioxide (CO₂) fluxes of grasslands. Hyperspectral reflectance data, CO₂ fluxes and biophysical parameters were measured at three grassland sites located in European mountain regions using standardized protocols. The relationships between CO₂ fluxes, ecophysiological variables, traditional VIs and VIs derived using all two-band combinations of wavelengths available from the whole hyperspectral data space were analysed. We found that VIs derived from hyperspectral data generally explained a large fraction of the variability in the investigated dependent variables but differed in their ability to estimate midday and daily average CO₂ fluxes and various derived ecophysiological parameters. Relationships between VIs and CO₂ fluxes and ecophysiological parameters were site-specific, likely due to differences in soils, vegetation parameters and environmental conditions. Chlorophyll and water-content-related VIs explained the largest fraction of variability in most of the dependent variables. Band selection based on a combination of a genetic algorithm with random forests (GA-rF) confirmed that it is difficult to select a universal band region suitable across the investigated ecosystems. Our findings have major implications for upscaling terrestrial CO₂ fluxes to larger regions and for remote- and proximal-sensing sampling and analysis strategies and call for more cross-site

synthesis studies linking ground-based spectral reflectance with ecosystem-scale CO₂ fluxes.

1 Introduction

Understanding the mechanisms that drive the carbon dioxide (CO₂) exchange of terrestrial ecosystems is one of the main challenges for ecologists working on climate change (Beer et al., 2010). Plant gross photosynthesis, also referred to as gross primary productivity (GPP), is one of the major components of the global carbon cycle. It interacts in complex ways with environmental factors such as radiation, nutrients, soil moisture, vapour pressure deficit, air temperature and soil temperature (Drolet et al., 2005). Plant biochemistry and structure determine many fundamental ecosystem patterns, processes and dynamics (Lambers et al., 1998; Waring and Running, 1998). The canopy nitrogen content regulates the canopy photosynthetic capacity and the canopy light use efficiency (ϵ) (Ollinger et al., 2008). In addition, the canopy chlorophyll content plays an important role in controlling ecosystem photosynthesis and carbon gain (Peng et al., 2011; Gitelson et al., 2006).

Optical remote sensing can help ecologists in qualitatively and quantitatively assessing plant and canopy properties (e.g. biomass – Vescovo et al., 2012; water content – Clevers et al., 2010; nitrogen content – Ollinger et al., 2008, Knyazikhin

et al., 2012; chlorophylls – Gitelson et al., 2006; and photosynthetic rate – Inoue et al., 2008) that drive ecosystem processes related to the carbon cycle.

Empirically and physically based methods have been proposed by several authors to interpret optical plant and canopy properties. Empirical methods consist of, for example, linear regression analysis between plant or canopy properties and optical data. The most widely used empirical methods are hyperspectral index methods (Peñuelas et al., 1993; Sims and Gamon, 2002; Inoue et al., 2008) and multivariable statistical methods, e.g. stepwise linear regression, genetic algorithm and neural network (Grossman et al., 1996; Riaño et al., 2005a; Li et al., 2007). Physical methods are based on the use of radiative transfer models (RTMs) to simulate light absorption and scattering through the canopy as a function of canopy structure and leaf biochemical composition (Jacquemoud et al., 2000; Zarco-Tejada et al., 2003). Therefore, RTMs help in quantifying the contribution of canopy biophysical and biochemical variables to canopy reflectance. Such models can be used for identifying regions of the light spectrum that are of particular importance for specific biophysical properties of vegetation. For example, it was demonstrated that the red-edge region (between 680 to 730 nm) of the spectrum is sensitive to the leaf chlorophyll content and leaf area index (LAI) (Baret et al., 1992). It is also well-accepted that an increase in LAI includes a decrease in reflectance in the red and an increase in the near-infrared (NIR) region (Jacquemoud, 1993). In the NIR region, effects of LAI and the leaf angle distribution equally contribute to the reflectance response (Bacour et al., 2002a). NIR reflectance between 800 and 850 nm is also related to canopy N content (Ollinger et al., 2008; Knyazikhin et al., 2012). In addition, the combination of the reflectance in NIR and in the short-wave infrared region (SWIR) is correlated with canopy water content (Colombo et al., 2008), but the reflectance between 1000 and 1400 nm is also highly sensitive to LAI. Therefore, some attention is needed when these spectral regions are used to retrieve water content, considering that the canopy properties in a given ecosystem often covary (Bacour et al., 2002b).

The drawback of such an approach consists in the fact that the process of building a model implies approximations and assumptions. For this reason we opted for a purely data-based approach such as the hyperspectral index approach. This method consists of the use of spectral vegetation indices (VIs) defined as spectral band ratios or normalized band ratios between the reflectance in the visible (VIS)-vs.-NIR, VIS-vs.-VIS or NIR-vs.-NIR region.

The typical optical sampling approach, which consists of linking spectral observations with CO₂ fluxes, is based on the Monteith (1972, 1977) equation:

$$\text{GPP} = \varepsilon \times \text{PAR} \times f_{\text{APAR}}, \quad (1)$$

where ε is the light use efficiency and f_{APAR} is the fraction of absorbed photosynthetically active radiation; both ε and

f_{APAR} can be retrieved by remote optical observations. A large number of VIs that can potentially be used to model the productivity of terrestrial ecosystems (as a proxy of ε and f_{APAR}) have been suggested (Inoue et al., 2008; Coops et al., 2010; Peñuelas et al., 2011; Rossini et al., 2012). The various VIs differ in their sensitivity to changes in photosynthetic status. “Greenness indices” – such the widely used normalized difference vegetation index (NDVI) – have been demonstrated to be a good proxy for f_{APAR} but are not sensitive to rapid changes in plant photosynthesis which are induced by common environmental and anthropogenic stressors (Gitelson et al., 2008; Hmimina et al., 2014; Soudani et al., 2014). However, in ecosystems characterized by strong dynamics (e.g. grasslands and crops with a strong green-up and senescence), other VIs are able to effectively monitor seasonal changes in biophysical parameters controlling canopy photosynthesis, such as f_{APAR} and chlorophyll content, and, consequently, can be adopted to monitor the seasonal and spatial variability of carbon fluxes (Gitelson et al., 2012; Sakowska et al., 2014). Short-term changes in ε can be remotely detected through a spectral proxy of the xanthophyll cycle (photochemical reflectance index, PRI; Gamon et al., 1992). The PRI is one of the most promising VIs for a direct estimation of photosynthetic light use efficiency and of its seasonal and diurnal variations (Nichol et al., 2002). Latest developments in the sun-induced fluorescence method may allow even more direct remote sensing of plant photosynthesis in the near future (Meroni et al., 2009; Rossini et al., 2010; Frankenberg et al., 2011). On the canopy scale, the relationship between PRI and ε was shown to be site-dependent (Garbulsky et al., 2011; Goerner et al., 2011) and strongly affected by environmental conditions (Soudani et al., 2014).

Whereas previous studies have demonstrated the ability of remote-sensing data to allow modelling ecosystem GPP on the ecosystem scale (e.g. Gianelle et al., 2009; Wohlfahrt et al., 2010; Rossini et al., 2012; Sakowska et al., 2014), a universal model for GPP estimation applicable across different ecosystems and a wide range of environmental conditions is still missing. Previous studies often focussed on single sites with specific characteristics (e.g. climate, vegetation composition, soil type; see Wohlfahrt et al., 2010). In addition, different studies often used different sensors, platforms and protocols (Balzarolo et al., 2011), making generalization difficult. Moreover, most of the studies have either relied on reflectance measurements in a few spectral wavebands (e.g. Wohlfahrt et al., 2010; Sakowska et al., 2014), missing potentially important information in under-sampled spectral regions. In order to overcome such heterogeneity in spectrometry measurements, SpecNet (<http://specnet.info>; Gamon et al., 2006), the European COST Action ES0903 (COST – Cooperation in Science and Technology; EUROSPEC; <http://cost-es0903.fem-environment.eu/>) and the COST Action ES1309 (OPTIMISE; http://www.cost.eu/domains_actions/essem/Actions/ES1309) focused on the definition of a stan-

Table 1. Description of the study sites and period.

| Site characteristics | Amplero | Neustift | Monte Bondone |
|--------------------------------|--------------------------|-------------------------------|--|
| Latitude | 41.9041 | 47.1162 | 46.0296 |
| Longitude | 13.6052 | 11.3204 | 11.0829 |
| Elevation (m) | 884 | 970 | 1550 |
| Mean annual temperature (°C) | 10.0 | 6.5 | 5.5 |
| Mean annual precipitation (mm) | 1365 | 852 | 1189 |
| Vegetation type | Seslerietum apenninae | Pastinaco– Arrhenatheretum | Nardetum Alpigenum |
| Study period* | 111–170, 2006 (9) | 122–303, 2006 (16) | 129–201, 2005 (13) 124–192, 2006 (12) |

* Range refers to days of the year (DOY); this is followed by the year; the number of hyperspectral measurement dates is given in brackets.

standardized protocol for making optical measurements at the eddy covariance CO₂ flux towers (Gamon et al., 2010).

The overarching objective of the present paper is thus to develop a common framework for predicting grassland carbon fluxes and ecophysiological parameters based on optical remote-sensing data across measurement sites exposed to diverse natural (climate) and anthropogenic (management) factors. To this end we combine eddy covariance CO₂ flux measurements with ground-based hyperspectral reflectance measurements for six different grasslands in Europe. In order to make the optical and fluxes measurements comparable, these were acquired at the six sites following a common protocol resulting in a unique standardized data set. We focused on European grasslands, which cover roughly 22 % (80 million ha) of the EU-25 land area and are thus among the dominating ecosystem types in Europe (EEA, 2005). Accordingly, their role in the European carbon balance has received a lot of scientific interest (Soussana et al., 2007; Gilmanov et al., 2007; Wohlfahrt et al., 2008; Ciais et al., 2010). Direct measurements of the grassland carbon exchange have been carried out and are still ongoing at a number of different grassland sites in Europe (e.g. Soussana et al., 2007; Cernusca et al., 2008). Scaling up these plot-level measurements to the continental scale requires a modelling approach typically based on or supported by remotely sensed data. Therefore, we believe that this study will improve the current knowledge on modelling the carbon dynamics of European grasslands.

2 Materials and methods

2.1 Experimental site description

This study was carried out at six experimental mountain grassland sites in Europe covering different climatic and grassland management conditions existing in the mountain regions of Europe, which were already part of the preceding study by Vescovo et al. (2012). This data set combined in situ hyperspectral, biophysical and flux measurements based on common protocol (for more details, see Sects. 2.2, 2.3

and 2.4). This data set is unique since no common protocol for hyperspectral measurements exists in the various eddy covariance networks (e.g. FLUXNET). In this study, three of these sites (Amplero, Neustift and Monte Bondone, see Tables 1 and S1 in the Supplement) composed the main data set used in the analysis, while the other three sites (Table S2) were used to independently validate the models obtained with the main data set.

Main study sites (Tables 1 and S1):

2.1.1 Amplero

The Amplero site is situated in the Mediterranean Apennine mountain region of Italy (41.90409° N, 13.60516° E) at 884 m a.s.l. This site is characterized by mild, rainy winters and by an intense drought in summer. Amplero is managed as a hay meadow, with one cut in late June and extensive grazing during summer and autumn (Balzarolo, 2008).

2.1.2 Monte Bondone

The Monte Bondone site is situated in the Italian Alps (46.01468° N, 11.04583° E) at 1550 m a.s.l. This site is characterized by a typical subcontinental climate, with mild summers and precipitation peaks in spring and autumn. Monte Bondone is managed as an extensive meadow, with one cut in mid-July.

2.1.3 Neustift

The Neustift grassland site is located in the Austrian Alps (47.11620° N, 11.32034° E) at 970 m a.s.l. The climate of this area is continental and Alpine, with precipitation peaks during the summer (July). This site is intensively managed as a hay meadow, with three cuts in mid-June, at the beginning of August and at the end of September.

Validation sites:

2.1.4 Längenfeld

The site Längenfeld is located in the Austrian Alps (47.0612° N, 10.9634° E) at 1180 m a.s.l. The climate of this area is continental/Alpine; however, compared to the other Alpine sites in this study, the site receives comparably less precipitation due to rain shadowing effects from both the north and south. The site is intensively managed as a hay meadow, with three cuts in mid-June, mid-August and mid-October.

2.1.5 Leutasch

The site Leutasch is located in the Austrian Alps (47.3780° N, 11.1627° E) at 1115 m a.s.l. The climate of this area is Alpine, with substantial precipitation due to its position on the north range of the Alps. The site is extensively managed as a hay meadow, with two cuts at the end of June and beginning of September.

2.1.6 Scharnitz

The site Scharnitz is located very close to Leutasch (47.3873° N, 11.2479° E) at 964 m a.s.l., and the climate is thus very similar to Leutasch. The site is extensively managed as a hay meadow, with two cuts at the beginning of July and beginning of September.

2.2 Hyperspectral reflectance measurements

The canopy hyperspectral reflectance measurements were collected at each site under clear-sky conditions close to solar noon (between 11:00 to 14:00 Central European Time) using the same model of a portable spectroradiometer (ASD Field-Spec HandHeld, Inc., Boulder, CO, USA) at all sites. The spectroradiometer acquires reflectance values between 350 and 1075 nm, with a full-width half maximum (FWHM) of 3.5 nm and a spectral resolution of 1 nm. In order to achieve a better match between the eddy covariance flux footprint and optical measurements, a cosine diffuser foreoptic (ASD Remote Cosine Receptor, Inc., Boulder, CO, USA), calibrated by the manufacturer, was used for nadir and zenith measurements (Gianelle et al., 2009; Fava et al., 2009; Meroni et al., 2011). The ASD's cosine receptor is designed with a geometry and material that provides a hemispherical field of view (FOV) of 180° and optimizes the cosine response. To reduce the nadir FOV contamination (i.e. sky irradiance and canopy irradiance) due to the hemispherical view of the sensor the instrument was placed on a 1.5 m long horizontal arm at a height of 1.5 m above the ground. To avoid the zenithal FOV contamination, the measurements were taken at least at a 15 m distance from the eddy covariance tower (maximum height of the tower was 6 m). The vegetation irradiance (sensor-pointing nadir) and sky irradiance (sensor-pointing

zenith) were measured by rotating the spectroradiometer alternately to acquire spectra from the vegetation and from the sky. Hemispherical reflectance was derived as the ratio of reflected to incident radiance. Each reflectance spectrum was automatically calculated and stored by the spectroradiometer as an average of 20 readings. Before starting each spectral sampling, a dark current measurement was done. For more details on the experimental set-up, see Vescovo et al. (2012). Spectral measurements were collected from spring until the cutting date at Amplero and Monte Bondone, while at the site in Neustift, which is cut three times during the season, spectral measurements were taken about once per week throughout the growing season of 2006.

2.3 Biophysical and biochemical canopy properties

Samples for dry phytomass, nitrogen and water content measurements were collected at the time of the hyperspectral measurements in the field of view of the hyperspectral sensor (see Vescovo et al., 2012 for more details). A similar data set was collected in 2013 at Monte Bondone by combining hyperspectral data with chlorophyll measurements. Chlorophyll samples were collected in the field of view of the hyperspectral sensor and chlorophyll content was detected by UV–VI spectroscopy. First, the samples were ground with liquid nitrogen and then immersed in 80 % acetone solution (0.1 g per 10 mL), shaken for 10 min in an automatic shaker at 250 rpm (Universal Table Shaker 709) and centrifuged at 4000 rpm for 10 min (Eppendorf 5810 R) in order to remove particles from the solution. The absorbance of extracted solutions was measured at 470, 646.8 and 663.2 nm by a UV–VIS spectrophotometer (Shimadzu UV-1601), and the concentrations of chlorophyll *a* (C_a), chlorophyll *b* (C_b) and carotenoids (C_{x+c}) were calculated as proposed by Lichtenthaler (1987). The weight of sampled sediment was used to calculate pigment concentrations per unit leaf mass (mg g^{-1}), and the weight of green biomass per ground area was used to obtain the total chlorophyll content (mg m^{-2}).

2.4 CO₂ flux measurements

Continuous measurements of the net ecosystem CO₂ exchange (NEE) were made by the eddy covariance (EC) technique (Baldocchi et al., 1996; Aubinet et al., 2012) at the six study sites using identical instrumentation. The three wind components and the speed of sound were measured using ultrasonic anemometers, and CO₂ molar densities were measured using open-path infrared gas analysers (IRGAs), as detailed in Tables S1 and S2. Raw data were acquired at 20 Hz and averaged over 30 min time windows in post-processing. Turbulent fluxes were obtained from raw data by applying block averaging (Monte Bondone, Neustift, validation sites) or linear de-trending (Amplero) methods with a time window of 30 min. A 3-D coordinate correction was performed according to Wilczak et al. (2001). The CO₂ fluxes

were corrected for, the effect of air density fluctuations as proposed by Webb et al. (1980). Low- and high-pass filtering was corrected for following Aubinet et al. (2000) (Amplero, Monte Bondone) or Moore (1986) (Neustift, validation sites). Data gaps due to sensors malfunctioning or violation of the assumptions underlying the EC method were removed and filled using the gap-filling and flux-partitioning techniques as proposed in Wohlfahrt et al. (2008). Ecosystem respiration (R_{eco}) was calculated from the y intercept of the light response model (see Eq. 4). Gross primary productivity (GPP) was calculated as the difference between NEE and R_{eco} . Half-hourly NEE and GPP values were averaged between 11:00 to 14:00 solar local time (at the time window of optical measurements) to allow for direct comparison with the hyperspectral data, and daily sums were also computed. At each site the following supporting environmental measurements were acquired: photosynthetically active radiation (PAR; quantum sensors), air temperature (T_a ; PT100, thermistor and thermoelement sensors) and humidity (RH; capacitance sensors) at some reference height above the canopy and soil temperature (T_s ; PT100, thermistor and thermoelement sensors) and volumetric water content (SWC; dielectric and time-domain reflectometry sensors) in the main rooting zone. In this study we used CO_2 flux and meteorological data of the years 2005 and 2006 for Monte Bondone and of 2006 for the other sites.

2.5 Estimation of grassland ecophysiological parameters

Canopy light use efficiency (ε) was derived from photosynthetically active radiation (PAR) absorbed by the canopy (APAR) as

$$\varepsilon = \frac{\text{GPP}}{\text{APAR}} = \frac{\text{GPP}}{\text{PAR} \times f_{\text{APAR}}} \quad (2)$$

and was estimated both at midday and daily time resolutions. We estimated the fraction of PAR absorbed by the canopy (f_{APAR}) from measured values of the leaf area index (LAI) using the Lambert–Beer law:

$$f_{\text{APAR}} = 0.95 \left(1 - e^{(-k \text{LAI})} \right), \quad (3)$$

where k is the canopy extinction coefficient (fixed at $k = 0.4$ as defined for a southern mixed-grass prairie in Texas; Kiniry et al., 2007) and 0.95 is the proportion of intercepted PAR that is absorbed by plants (Schwalm et al., 2006). LAI was quantified non-destructively by an indirect method based on canopy PAR transmission using line PAR sensors (SunScan, Delta-T, UK) and an inversion of an RTM (Wohlfahrt et al., 2001). These measurements were done within the footprint area of the spectroradiometer simultaneously with the hyperspectral measurements.

Three additional key parameters of the response of NEE to PAR were extracted by fitting measured NEE and PAR to

a simple Michaelis–Menten-type model:

$$\text{NEE} = \frac{-\alpha \text{PAR} F_{\text{sat}}}{\alpha \text{PAR} + F_{\text{sat}}} + R_{\text{eco}}, \quad (4)$$

where α represents the apparent quantum yield ($\mu\text{mol CO}_2 \mu\text{mol}^{-1}$ photons), F_{sat} the asymptotic value of GPP ($\mu\text{mol CO}_2 \text{m}^{-2} \text{s}^{-1}$), PAR the photosynthetically active radiation ($\mu\text{mol photons m}^{-2} \text{s}^{-1}$) and R_{eco} the ecosystem respiration ($\mu\text{mol CO}_2 \text{m}^{-2} \text{s}^{-1}$). For all sites, using the Levenberg–Marquardt (Marquardt, 1963) algorithm the parameters of Eq. (4) were estimated by fitting Eq. (4) to both day and nighttime data, which were pooled into 3-day blocks centred on the date of the hyperspectral data acquisition. For each acquisition date, we then used Eq. (3) to derive GPP at an incident PAR of $1500 \mu\text{mol m}^{-2} \text{s}^{-1}$, referred to as GPP_{max} in the following.

2.6 Hyperspectral data analysis

In order to explore the information content of the hyperspectral data for estimating CO_2 fluxes (i.e. midday and daily average of NEE and GPP) and ecophysiological parameters (i.e. α , ε and GPP_{max}), we performed a correlation analysis between spectral reflectance indices (independent variables) and these (dependent) variables. To this end, we derived spectral ratio (SR; Eq. 5), spectral difference (SD; Eq. 6) and normalized spectral difference (NSD; Eq. 6) indices using all possible two-band (i and j) reflectance (ρ) combinations between 400 and 1000 nm (180 600 combinations). These three formulations were selected since they represent the most common equations used to compute vegetation indices (see Table 2).

$$\text{SR}_{i,j} = \frac{\rho_i}{\rho_j} \quad (5)$$

$$\text{SD}_{i,j} = \rho_i - \rho_j \quad (6)$$

$$\text{NSD}_{i,j} = \frac{\rho_i - \rho_j}{\rho_i + \rho_j} \quad (7)$$

Linear regression analysis was performed among all possible wavelength combinations for all three index types (SR, NSD and SD) and the investigated dependent variables.

The performance of linear models in predicting dependent variables (i.e. carbon fluxes and ecophysiological parameters) was evaluated by the coefficient of determination (R^2) and root mean square error (RMSE). The coefficients of determination (R^2) resulting from the linear models were visualized in correlograms, as in the example in Fig. 1.

We also calculated four SR and seven NSD indices which are commonly used in relation to vegetation activity and CO_2 fluxes (Table 2). Figure 1 shows the location of these indices in the waveband space of the correlograms. In this analysis, we also considered the enhanced vegetation index (EVI), which is one of the most frequently used vegetation indices to predict CO_2 fluxes. In Fig. 1 the location of the EVI is not

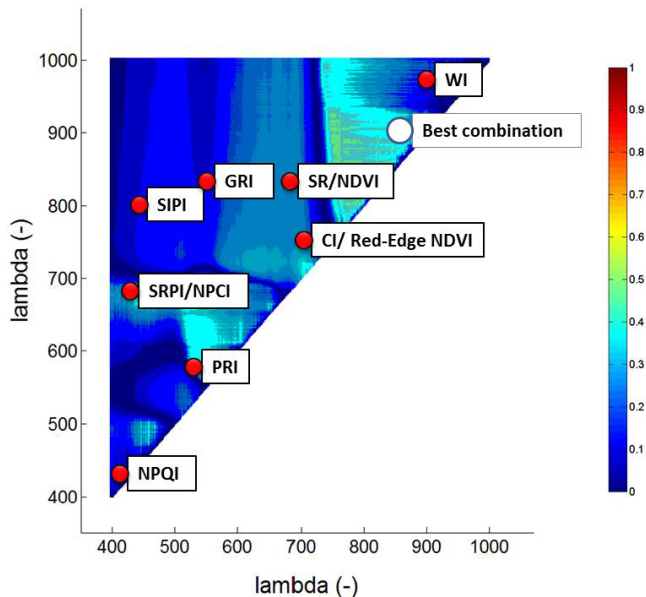


Figure 1. A selected example of a correlogram between NSD-type indices and midday average GPP for all sites pooled. The correlogram shows all R^2 values, the white dot indicates the two-band combination with the highest R^2 value and the red dots indicate the location of the reference VIs reported in Table 2 (SR: simple ratio; GRI: green ratio index; WI: water index; SRPI: simple ratio pigment index; NDVI: normalized difference vegetation index; NPQI: normalized phaeophytinization index; NPCI: normalized pigment chlorophyll index; CI: chlorophyll index; red-edge NDVI; SIPI: structural independent pigment index; PRI: photochemical reflectance index).

shown since this index is computed by the combination of three spectral bands as shown in Table 2.

The robustness of the model selected on the basis of the best band combinations for all ecophysiological parameters for each site and all sites pooled was tested by the leave-one-out cross-validation technique. The predictive performance was expressed as the cross-validated coefficient of determination (R_{CV}^2) and the cross-validated root mean square error ($RMSE_{CV}$). In addition, the capability of the selected models in predicting different ecophysiological parameters was tested by applying the selected models to the validation data set (Table S2) composed of three different grasslands not used in the previous analysis. This data set was selected because the hyperspectral and flux data were collected by using exactly the same protocol applied for the main data set (see Sect. 2.1).

In order to explore the basis of the correlation between the selected band combinations and ecophysiological variables (e.g. α , GPP_{max} , GPP , ϵ), the relationship between the selected bands and biophysical parameters such as dry phytomass, nitrogen and water content collected during the field campaign in the same footprint of the hyperspectral measurements was examined.

2.7 Band selection based on the combination of random forests and genetic algorithm (GA-rF)

In order to complement the more conventional analysis described in the previous section, we also explored the use of a hybrid feature selection strategy based on a genetic algorithm and random forests (GA-rF). The first method was used for the feature selection and the second one as regression for predicting the target variables. First of all, the original data set was aggregated to 10 nm bands in order to reduce the effects of autocorrelation in frequency space. The algorithm generates a number of possible model solutions (chromosomes) and uses these to evolve towards an approximation of the best solution of the model. In our case the genes of each chromosome correspond to the wavebands. We made use of five genes for each chromosome in order to overcome overfitting. Each population of 1000 chromosomes evolved for 200 generations. The mutation chance was set to the inverse of a population size increase of 1. The fitness of each chromosome was measured by applying the random forest algorithm (Breiman, 2001). This was used as an ensemble method for regression that is based on the uncontrolled development of decision trees ($n = 100$). We opted for this method because of its demonstrated efficiency with large data sets. In combining the two methods, we choose the mean squared error as the target variable to be minimized.

3 Results

3.1 Seasonal variation of meteorological variables, LAI and CO_2 fluxes

Environmental conditions and the seasonal development of LAI, NEE, GPP_{α} , ϵ and GPP_{max} during the study period are shown in Fig. 2. A strong influence of the typical climatic conditions at the three study sites was evident: Amplero was characterized by a Mediterranean climate, with highest incoming radiation and temperatures and the lowest amount of precipitation, which translated into a substantial seasonal drawdown of soil moisture. Monte Bondone and Neustift, more influenced by a continental Alpine climate, experienced comparably lower temperatures with higher precipitation and soil moisture with respect to Amplero (Fig. 2).

Maximum LAI values were similar at Monte Bondone and Amplero ($2.8\text{--}3.4\text{ m}^2\text{ m}^{-2}$), while twice as much leaf area developed at the more intensively managed study site Neustift. The latter was also characterized by higher NEE and GPP (i.e. more photosynthesis and net uptake of CO_2). The reductions in leaf area related to the cuts of the grasslands were associated, as expected, with marked increases and reductions in NEE and GPP, respectively. The canopy light use efficiency, ϵ , was inversely related to GPP and LAI, peaking at the beginning of the season at Amplero and Monte Bondone ($0.01\text{--}0.10\ \mu\text{mol photons}\ \mu\text{mol}^{-1}\ CO_2$),

Table 2. Summary of the vegetation indices characteristics used in this study.

| Index name and acronym | Formula | Use | Reference |
|---|---|---|------------------------------|
| Simple spectral ratio indices | | | |
| Simple ratio (SR or RVI) | $SR = R_{830}/R_{660}$ | Greenness | Jordan (1969) |
| Green ratio index (GRI) | $GRI = R_{830}/R_{550}$ | Greenness | Peñuelas and Filella (1998) |
| Water index (WI) | $WI = R_{900}/R_{970}$ | Water content, leaf water potential, canopy water content | Peñuelas et al. (1993) |
| Simple ratio pigment index (SRPI) | $SRPI = (R_{430})/(R_{680})$ | Carotenoid/chlorophyll ratio | Peñuelas et al. (1995) |
| Chlorophyll index (CI) | $CI = (R_{750}/R_{720}) - 1$ | Chlorophyll content | Gitelson et al. (2005) |
| Normalized spectral difference vegetation indices | | | |
| Normalized difference vegetation index (NDVI) | $NDVI = (R_{830} - R_{660}) / (R_{830} + R_{660})$ | Greenness | Rouse et al. (1973) |
| Normalized phaeophytinization index (NPQI) | $NPQI = (R_{415} - R_{435}) / (R_{415} + R_{435})$ | Carotenoid/chlorophyll ratio | Barnes et al. (1992) |
| Normalized pigment chlorophyll index (NPCI) | $NPCI = (R_{680} - R_{430}) / (R_{680} + R_{430})$ | Chlorophyll ratio | Peñuelas et al. (1994) |
| Red-edge NDVI | $NDVI_{RedEdge} = (R_{750} - R_{720}) / (R_{750} + R_{720})$ | Chlorophyll content | Gitelson and Merzlyak (1994) |
| Structural independent pigment index (SIPI) | $SIPI = (R_{800} - R_{445}) / (R_{800} + R_{445})$ | Chlorophyll content | Peñuelas et al. (1995) |
| Photochemical reflectance index (PRI) | $PRI = (R_{531} - R_{570}) / (R_{531} + R_{570})$ | Photosynthetic light use efficiency (and leaf pigment contents) | Gamon et al. (1992) |
| Improved for soil and atmospheric effects | | | |
| Enhanced vegetation index (EVI) | $EVI = 2.5 (R_{830} - R_{660}) / (1 + R_{830} + 6 R_{660} - 7.5 R_{460})$ | Vegetation index improved for soil and atmospheric effects | Huete et al. (1997) |

while for Neustift ε showed the highest values after the cuts (0.01–0.20 $\mu\text{mol photons } \mu\text{mol}^{-1} \text{CO}_2$). At Amplero, α and GPP_{max} peaked in spring and then decreased during the summer drought period, while at Neustift and Monte Bondone, temporal patterns of α and GPP_{max} were more strongly affected by management.

3.2 Hyperspectral data and their relation to CO₂ fluxes and ecophysiological parameters

Figures 3–5 show correlograms between NSD-, SR- and SD-type indices, respectively, and the investigated dependent midday ecophysiological parameters and fluxes. The correlograms for daily data can be found in the Supplement (Figs. S2–S4 in Supplement). Selected examples of key spectral signatures of the investigated grasslands are shown in Fig. S1 in the Supplement.

A number of interesting insights may be gained from Figs. 3–5 and S2–S4, which we summarize in the following:

1. The correlograms exhibited quite different patterns – some correlograms showed that a wide range of band combinations was able to explain the simulated quanti-

ties (e.g. GPP at Amplero; Figs. 3 and S2), while some correlograms exhibited very pronounced patterns, with the R^2 value changing greatly with subtle changes in band combinations (e.g. ε at Neustift; Figs. 3 and S2).

2. Maximum R^2 values were often clearly higher than the surrounding areas of high predictive power (e.g. ε at Amplero; Fig. 3).
3. The different types of indices (compare Figs. 3–5) yielded similarly high correlations with the same dependent variable at the same site in similar spectral regions. This indicates that band selection is more important for explanatory power than the mathematical formulation of the VI (i.e. ratio vs. difference, with/without normalization). SR and NSD indices (Figs. 3 and 4) yielded similar results compared to SD indices (Fig. 5).
4. The highest correlations for all dependent variables were found either for indices combining bands in the visible range (VIS: < 700 nm) or the red edge and NIR (NIR: > 700 nm), corresponding to spectral regions used by indices such as the SRPI, NPCI, PRI and

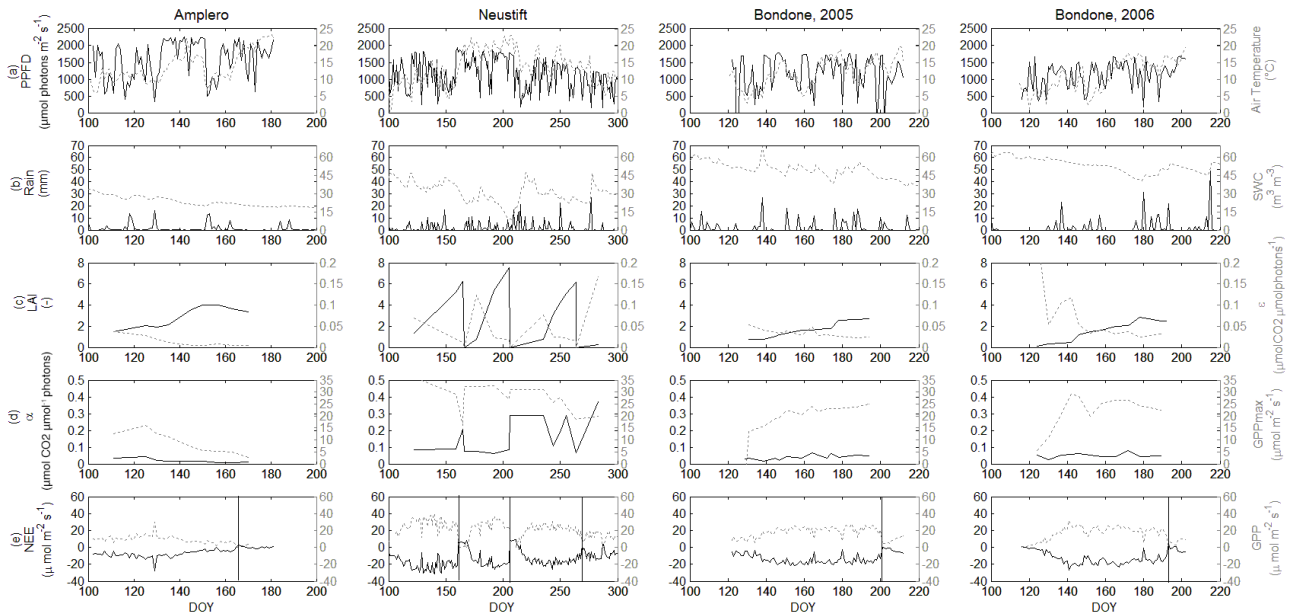


Figure 2. Seasonal variation of meteorological variables, LAI, CO_2 fluxes and ecophysiological parameters for the period of the hyperspectral measurements at the three investigated grasslands. **(a)** Midday average photosynthetically active radiation (PAR; $\mu\text{mol m}^{-2} \text{s}^{-1}$; solid black line) and daily average air temperature ($^{\circ}\text{C}$; dotted grey line); **(b)** daily precipitation (Rain; mm; solid black line) and daily average soil water content (SWC; $\text{m}^3 \text{m}^{-3}$; dotted grey line); **(c)** leaf area index (LAI; $\text{m}^2 \text{m}^{-2}$; solid black line) and light use efficiency (ϵ ; $\mu\text{mol photons } \mu\text{mol}^{-1} \text{CO}_2$; dotted grey line); **(d)** apparent quantum yield (α ; $\mu\text{mol CO}_2 \mu\text{mol}^{-1} \text{photons}$; solid black line) and gross primary production at saturating light (GPP_{max} ; $\mu\text{mol m}^{-2} \text{s}^{-1}$; dotted grey line); **(e)** midday average net ecosystem CO_2 exchange (NEE; $\mu\text{mol m}^{-2} \text{s}^{-1}$; solid black line) and gross primary production (GPP; $\mu\text{mol m}^{-2} \text{s}^{-1}$; grey dotted line); vertical lines in the lowermost panels indicate the dates of mowing.

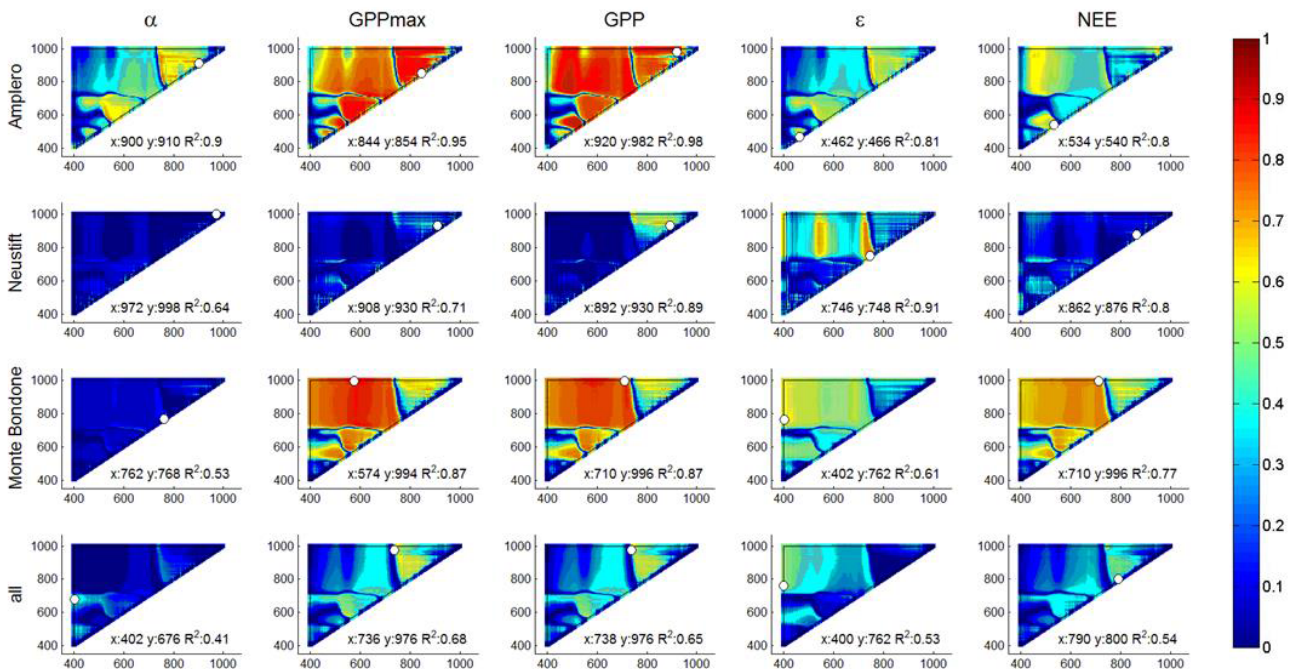


Figure 3. Correlograms of R^2 values for α , GPP_{max} , midday averaged GPP, ϵ and NEE, on the one hand, and NSD-type indices for Amplero, Neustift, Monte Bondone (both study years pooled) and all sites pooled on the other. The white dots indicate the position of paired band combinations corresponding to the maximum R^2 .

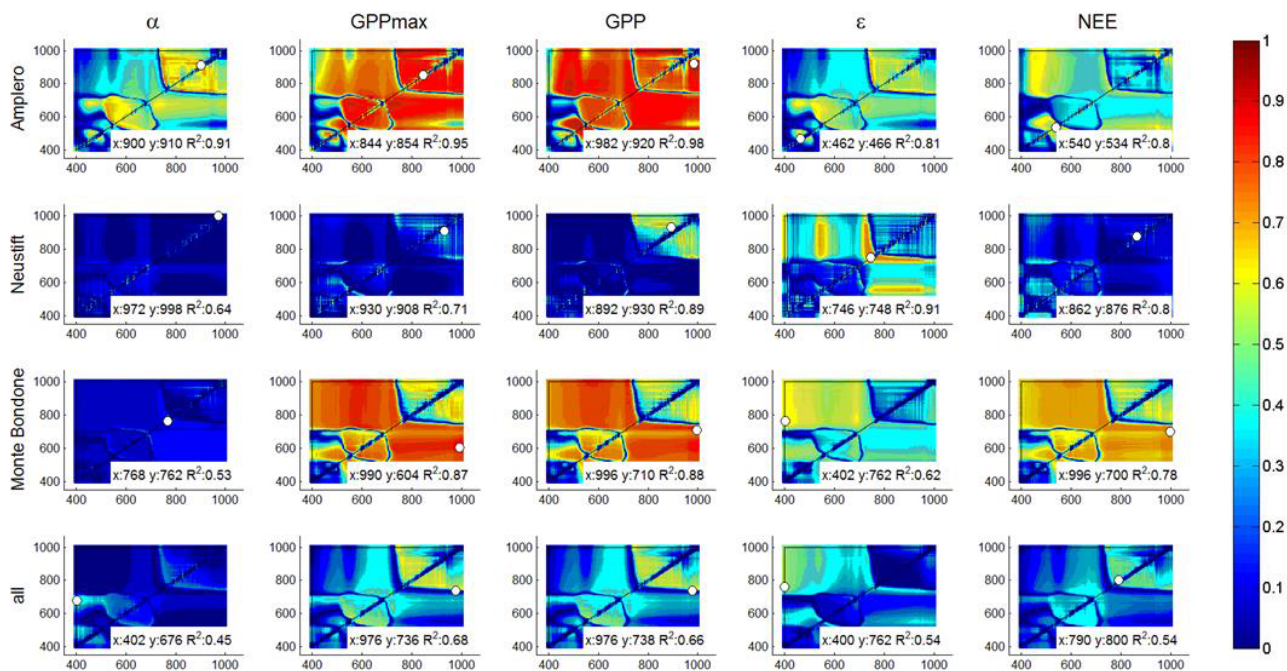


Figure 4. Correlograms of R^2 values for α , GPP_{max} , midday averaged GPP, ϵ and NEE, on the one hand, and SR-type indices for Amplero, Neustift, Monte Bondone (both study years pooled) and all sites pooled on the other. The white dots indicate the position of paired band combinations corresponding to the maximum R^2 .

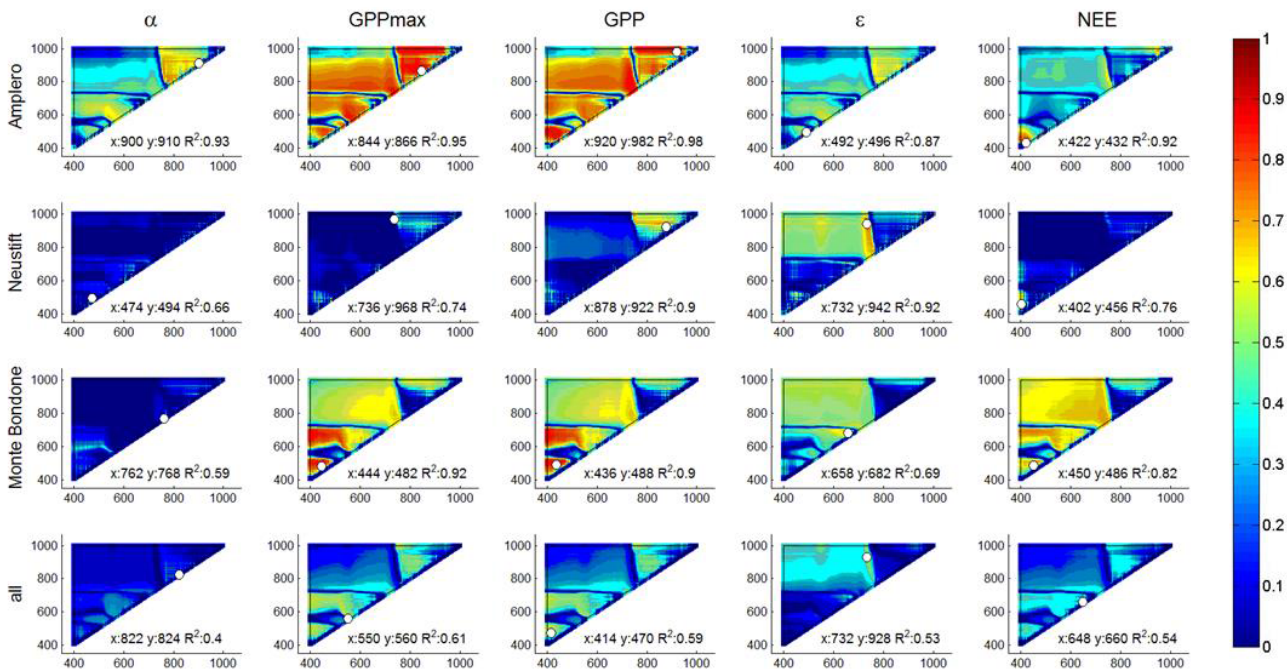


Figure 5. Correlograms of R^2 values for α , GPP_{max} , midday averaged GPP, ϵ and NEE, on the one hand, and SD-type indices for Amplero, Neustift, Monte Bondone (both study years pooled) and all sites pooled on the other. The white dots indicate the position of paired band combinations corresponding to the maximum R^2 .

NPQI, and the CI and WI, respectively. Spectral regions of well-known indices, such as NDVI, SR, SIPI or GRI,

which exploit the contrasting reflectance magnitudes in

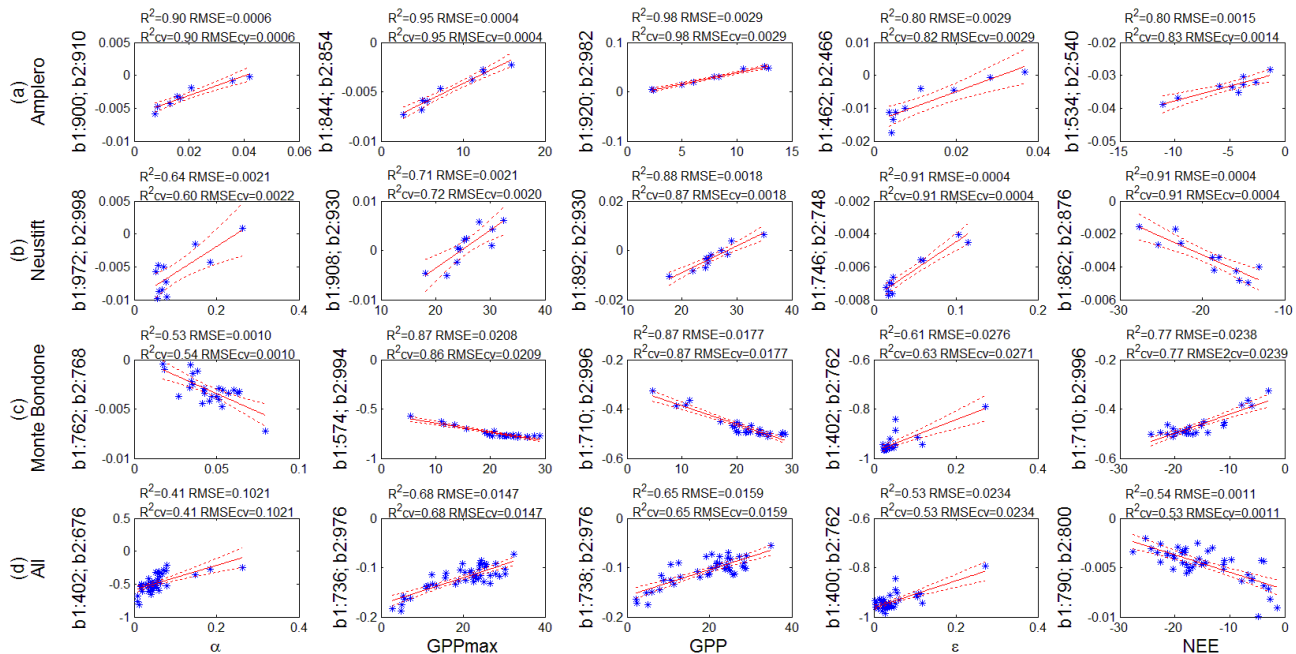


Figure 6. Results of linear correlation analysis for α , GPP_{max} , midday averaged GPP, ε and NEE, on the one hand, and selected best NSD-type indices for (a) Amplero, (b) Neustift, (c) Monte Bondone (both study years pooled) and (d) all sites pooled on the other. R^2 – coefficient of determination; RMSE – root mean square error; R^2_{cv} – cross-validated coefficient of determination; $RMSE_{cv}$ – cross-validated root mean square error. The solid red lines indicate the fitted models, and the dotted red lines represent the 95 % upper and lower confidence bounds.

the visible and NIR (Fig. S1), resulted in comparably lower correlations.

- For midday and daily time resolutions different band combinations were selected (e.g. NEE at Amplero; compare Figs. 4 and S3). For similar selected regions, daily averages were characterized by higher explanatory power compared to midday averages (e.g. ε at Neustift).

Figure 6 shows the performance of linear regression models for the best NSD-type indices for midday ecophysiological parameters for each site and all sites pooled (Fig. S7 shows the results of the same analysis for daily averages). Large differences existed between the study sites regarding the explanatory power of the same index for the same dependent variable. The highest R^2_{cv} and values were generally obtained for Amplero, followed by Neustift and then Monte Bondone, and the lowest R^2_{cv} values resulted when data from all three sites were pooled, confirming the difficulties in finding a general relation valid among sites.

For Amplero and Neustift the NIR-vs.-NIR combinations showed a positive linear regression model with α , GPP_{max} and GPP, while for Monte Bondone a negative linear correlation was observed. For Amplero the VIS-vs.-VIS combination showed a good performance in predicting ε ; the NIR-vs.-NIR combinations showed good performance for Neustift, as did the VIS-vs.-NIR combination for Monte Bondone. The linear models for NEE were site-specific. In fact, Amplero and Monte Bondone showed a positive linear regres-

sion model for NEE, but the VIS-vs.-VIS band combination was selected for Amplero and the NIR-vs.-NIR combination for Monte Bondone. Neustift performed well with NEE for NIR-vs.-NIR combinations, but with an inverse relationship.

The different types of indices (compare Figs. 6, S5 and S6) resulted in similar models. The different time resolutions gave different models (e.g. GPP, ε and NEE at Monte Bondone; compare Figs. 6 and S7, Figs. S5 and S8, or Figs. S6 and S9).

3.3 Correlation between conventional VIs, ecophysiological variables and CO_2 fluxes

The correlation analysis between the conventional VIs, the midday CO_2 fluxes (Table 3) and ecophysiological parameters (Table 4), generally confirmed the results obtained with the hyperspectral data.

For the same dependent variable (α , GPP_{max} , GPP, ε and NEE), the performance of the various VIs showed large differences between sites. For example, for GPP_{max} all of the investigated indices except NPQI resulted in significant linear correlations at Amplero, explaining 41–89 % of the variability in GPP_{max} . In contrast, only NDVI, PRI, NPCI and SRPI showed a slightly significant linear performance (17–26 %) for GPP_{max} at Neustift.

The different VIs performed differently in predicting the same dependent variable at the different study sites. For all dependent variables (Tables 3, 4 and S3), the VI resulting in

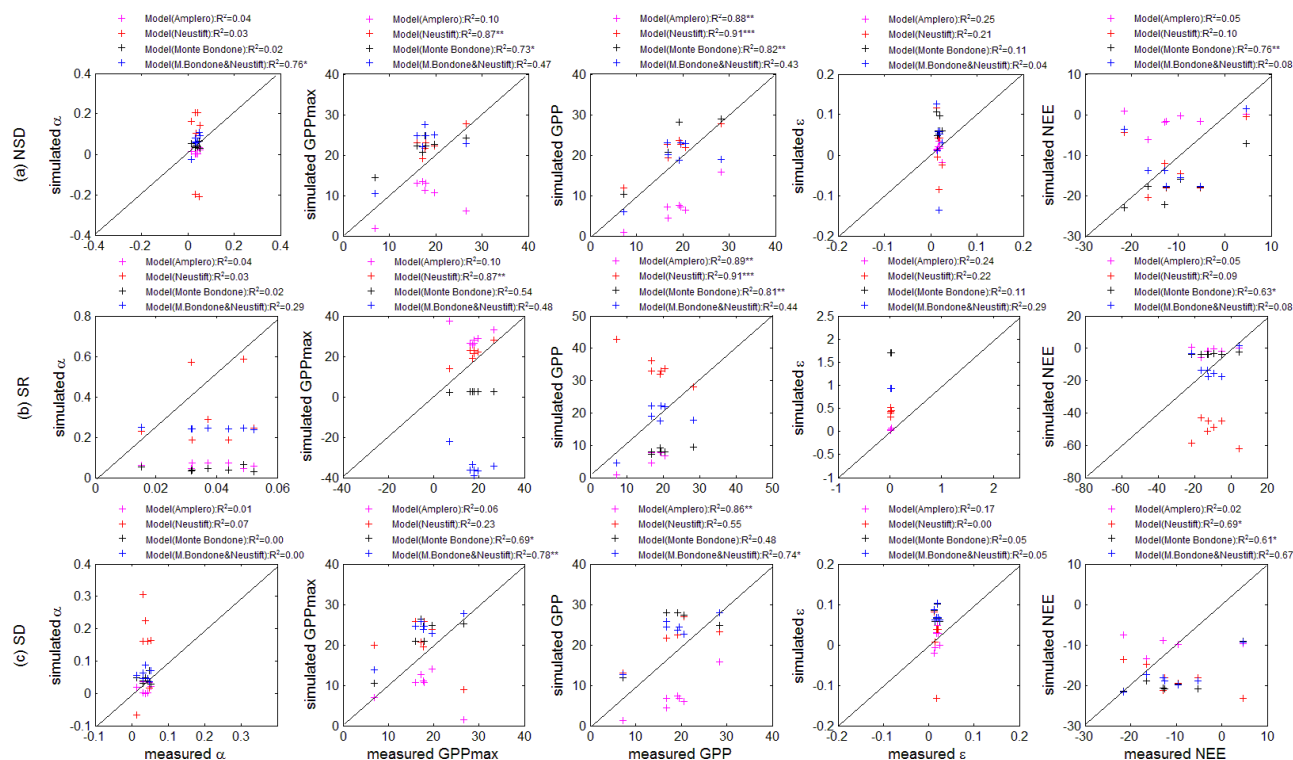


Figure 7. Results of validation of linear regression models between VIs (**(a)** NSD-type; **(b)** SR-type; **(c)** SD-type) and ecophysiological parameters: α , ϵ (midday average), GPP_{max} and midday average CO_2 fluxes (NEE and GPP). R^2 – coefficient of determination. Different colours represent results of the validation performed applying to the three new sites the model for Amplerio (in magenta), Neustift (in red) and Monte Bondone (in blue) and a model-parameterized grouping Monte Bondone and Neustift (M.Bondone&Neustift; in black). Statistical significance is indicated as * ($p < 0.05$), ** ($p < 0.01$) and *** ($p < 0.001$). The black lines are 1 : 1 lines.

the highest R^2 values was never the same at all sites. Often the best-fitting VI at one site resulted in a non-significant correlation at another site. Therefore, none of the dependent variables clearly emerged as the one best predicted (Tables 3, 4 and S3).

When data from all sites were pooled, models showed the same performance for the same VI and dependent variable except for GPP and NEE. The best-performing VI for GPP and NEE was SIPI; NPCI performed best for α , GRI for ϵ and SIPI for GPP_{max} .

The choice of the averaging period (midday vs. daily) applied to ϵ , NEE and GPP generally did not modify the ranking of the VIs, but the R^2 values tended to be similar or somewhat higher on the daily timescale (compare Tables 3 and 4 with Table S3).

3.4 Evaluation of the model performance

Figure 7 shows the results of the validation for each ecophysiological parameter and midday averaged fluxes and NSD-, SR- and SD-type indices against data from the validation sites. The models used in the validation are based on the best models determined for each site (i.e. Amplerio, Neustift and Monte Bondone) and on pooling together the two alpine

grasslands of Monte Bondone and Neustift (referred to as M.Bondone&Neustift).

Overall, the results of the validation were mixed. Good performance was observed mainly for the Neustift, Monte Bondone and pooled M.Bondone&Neustift models (see Table S4). In particular, the best performance values were obtained for (i) α for the pooled Monte Bondone and Neustift model for SR-type indices; (ii) GPP_{max} for NSD-, SR- and SD-type indices and models except for Amplerio; and (iii) for midday GPP for all NSD-, SR- and SD-type indices and models. It is interesting to note that lower performances were generally found for the models based on the Amplerio parameterization. This is understandable as Monte Bondone and in particular Neustift were structurally and functionally much more similar to the validation sites compared to Amplerio (Tables 1 and S2). Considerably poorer performance was observed for ϵ and NEE across all model–index type combinations (Table S4). The validation on a daily timescale always resulted in a poorer performance compared to the midday average timescale (Fig. S10 and Table S5).

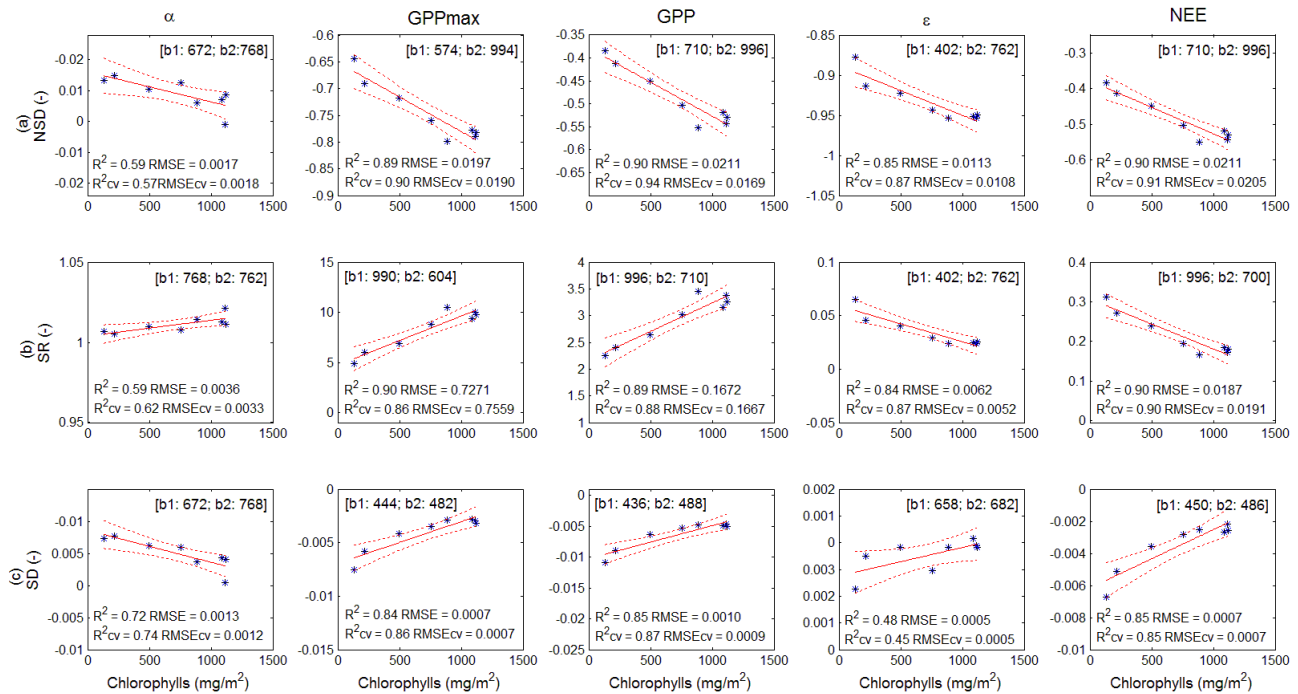


Figure 8. Correlation between selected (a) NSD-, (b) SR- and (c) SD-type indices for the α , GPP_{max} , midday GPP, midday ϵ and midday NEE (plots in the columns) and the total chlorophyll content for Monte Bondone in 2013. R^2 – coefficient of correlation; RMSE – root mean square error; R^2_{cv} – cross-validated coefficient of correlation; $RMSE_{cv}$ – cross-validated root mean square error. The solid red lines indicate the fitted models, and the dotted red lines represent the 95 % upper and lower confidence bounds. The selected bands for computing NSD-, SR- and SD-type indices are reported in brackets.

3.5 Effects of canopy structure on selected band combinations

Tables 5 and S6 show the results of the correlation analysis between the selected NSD-, SR- and SD-type indices for ecophysiological variables and fluxes and biophysical properties of vegetation, such as dry phytomass, nitrogen and water content. Overall, the spectral response in the selected band combinations for NSD-, SR- and SD-type indices was strongly related to vegetation properties of the three grasslands (e.g. nitrogen and dry phytomass), which impacted on their spectral response in the NIR and VIS regions. For the Mediterranean site (Amplero) and for all ecophysiological parameters (e.g. α , GPP_{max}), dry phytomass was the main driving factor of the spectral response in the selected bands, while nitrogen content drove the spectral response in the NIR region for Neustift. For Monte Bondone, both dry phytomass and nitrogen content affected the spectral response of the grassland. Similar results were obtained for SR- and SD-type indices.

Figures 8 and S11 show the correlation analysis between the selected NSD-, SR- and SD-type indices for all ecophysiological parameters (e.g. α , GPP_{max}) and chlorophyll content for Monte Bondone in 2013. The chlorophyll content showed a very good correlation for all selected models and for all indices. The values of R^2 were always higher than the

values of R^2 obtained for the other biophysical variables (Tables 5 and S6). In Fig. 9, it is possible to see that NSD- and SR-type indices for the selected bands for estimating GPP (i.e. 996 and 710 nm) are strongly correlated with canopy-total chlorophyll content ($R^2 > 0.80$).

3.6 Band selection using the GA-rF method

Figure 9 shows the results of the band selection based on the GA-rF method. In particular, each plot represents the frequency of the occurrence of each band in the genetic algorithm.

Overall, using the GA-rF method it was possible to identify portions of the spectrum that were of particular significance for estimating specific properties of the different ecosystems. For example, for predicting midday GPP (Fig. 9b) for all sites pooled together, the bands at 430, 630, 660 and 710 nm showed the best results. The bands at 505 nm, 660 nm and 710 nm played an important role in predicting midday GPP for Amplero, Neustift and Monte Bondone, respectively. Some differences were found for the different time resolutions (compare Fig. 9b and c). For example, the bands at 580 and 800 nm showed the best results for Amplero, and bands at 530 nm showed the best results for Neustift.

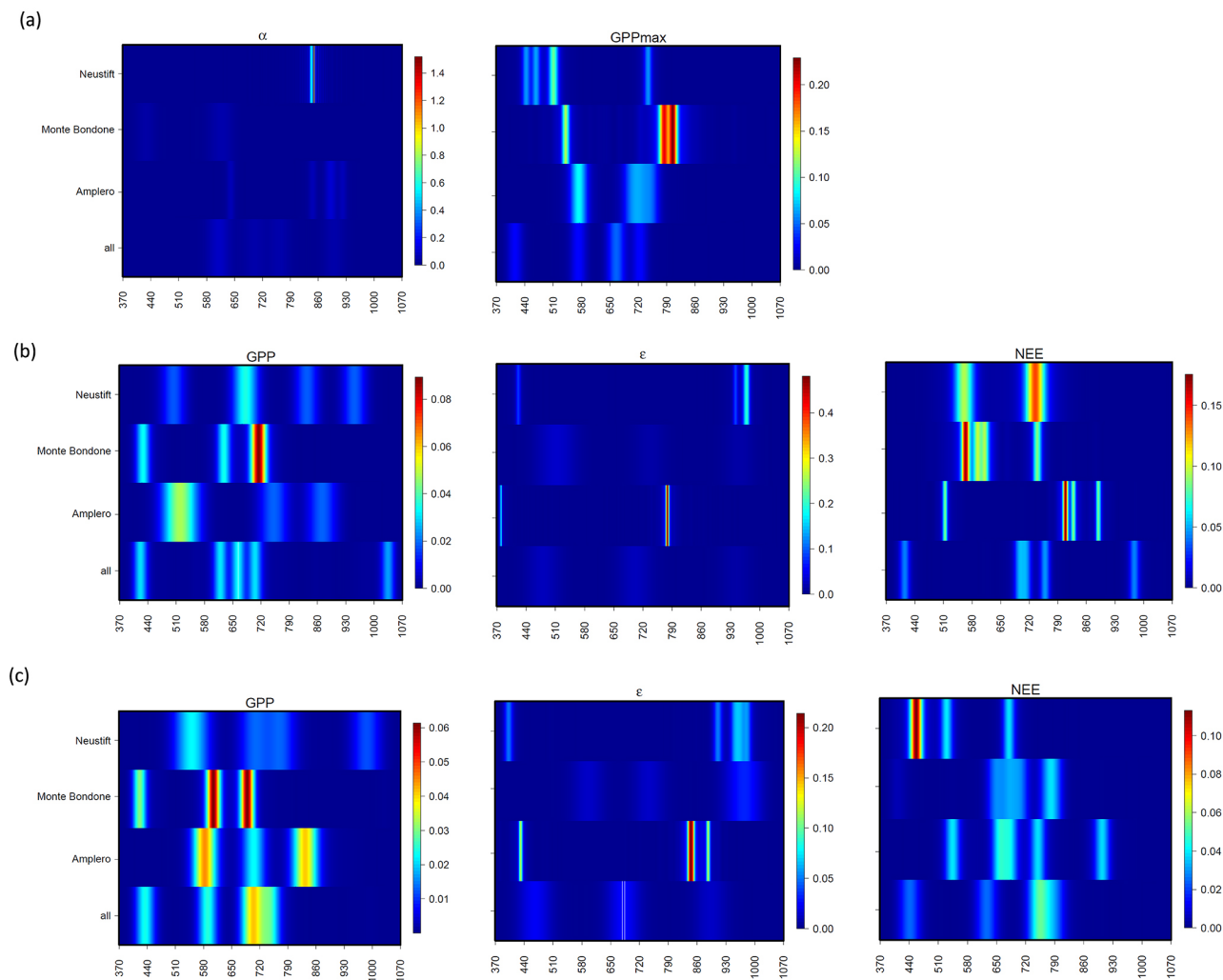


Figure 9. Results of the GA-rF method for band selection for Amplero, Neustift, Monte Bondone and all sites pooled for (a) α and GPP_{max} , (b) midday average ε and CO_2 fluxes (NEE and GPP); (c) daily average ε and CO_2 fluxes (NEE and GPP).

Figure 10 shows the results for the band selection by GA-rF methods for biophysical variables (i.e. dry phytomass, nitrogen and water content). For the variables related to slow processes, the GA-rF method highlighted different bands for different sites; a much higher between-site variability for the variables related to ecophysiological processes (e.g. ε , α and GPP_{max}) was detected, and we weren't able to identify common "hot spots".

4 Discussion

This study aimed at evaluating the potential of hyperspectral reflectance measurements to simulate CO_2 fluxes and ecophysiological variables of European mountain grasslands over a range of climatic conditions and management practices (grazing, harvest). To this end, we combined eddy covariance CO_2 flux measurements with ground-based hyper-

spectral measurements at six mountain grassland sites in Europe.

4.1 Upscaling of in situ relationships between VI indices and CO_2 fluxes and ecophysiological parameters

Despite the fact that we focused on a single type of ecosystem, our results showed that large differences existed among the investigated sites in the relationships between hyperspectral reflectance data and CO_2 fluxes and ecophysiological parameters. For all study sites pooled, hyperspectral reflectance data explained 40–68 % of the variability in the dependent variables (Figs. 3–5). The conventional VIs yielded a maximum of 47 % of explained variability in the data (Tables 3–4).

This is the first study comparing different grasslands characterized by different plant species and environmental con-

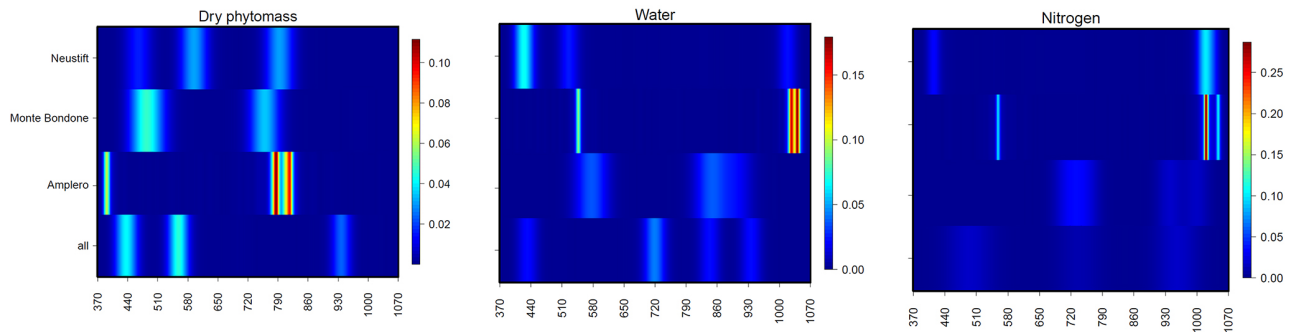


Figure 10. Results of the GA-rF method for band selection for Amplerlo, Neustift, Monte Bondone and all sites pooled for dry phytomass, water and nitrogen content.

ditions. The use of simple models based on a linear relationship between GPP and VIs, related to canopy greenness, has proven to be a good proxy for the GPP of ecosystems with strong green-up and senescence (Peng et al., 2011; Rossini et al., 2012). The loss of this relationship may be related to low ε variability due to abiotic and biotic stressors, the dependency of PRI on LAI, leaf and canopy biochemical structure (e.g. leaf orientation), and xanthophyll cycle inhibition or saturation, and zeaxanthin-independent quenching (Gamon et al., 2001; Filella et al., 2004; Rahimzadeh-Bajgiran et al., 2012; Hmimina et al., 2014). For alpine grasslands, a key meteorological variable that played a relevant role in stimulating ε was high soil water content associated with low temperatures (Polley et al., 2011). Low soil water contents also triggered a decrease in leaf conductance as well as in ε and in α for two oak and beech ecosystems (Hmimina et al., 2014). However, no significant differences in leaf biochemical and structural properties of the canopy at the lowest and highest water content were found. In addition, in this special issue, Sakowska et al. (2014) showed that ε is also strongly affected by the directional distribution of incident PAR, i.e. the ratio of direct to diffuse PAR.

Considering all sites pooled together (Figs. 3 and S2), NSD-type indices showed a very poor correlation in the VIS-vs.-NIR band combinations (i.e. traditional greenness indices; see Table 2) with GPP. It is well-known in the literature (Rossini et al., 2010, 2012; Peng et al., 2010; Sakowska et al., 2014) that greenness indices, for grasslands and crops, are often good proxies of $f_{\text{APARgreen}}$ (and thus carbon fluxes). Interestingly, in our study their performance was considerably poorer than expected. The NSD-type index showed a better performance in VIS-vs.-VIS band combinations than VIS-vs.-NIR ones. VIS-vs.-VIS band combinations for NSD-type indices (e.g. green vs. blue or red and green vs. green wavelengths; see, e.g., Inoue et al., 2008) are defined as greenness indices (Fig. 1), although their performance is generally much poorer than NSD VIS-vs.-NIR indices. These results are likely due to the confounding effects of the different canopy structures and consequently of the different

NIR response of the investigated grasslands (see Fig. S1). In fact, the different grassland structures (spatial distribution of photosynthetic and also non-photosynthetic material, leaf angles, etc.) affect our ability to use traditional indices to estimate $f_{\text{APARgreen}}$ (and fluxes) when we consider different grasslands together because the structural effects on scattering are very complex in the NIR (Jacquemoud et al., 2009; Knyazikhin et al., 2012). These results are of importance for the community, which still relies on these relationships a lot, also favoured by the availability of affordable narrow-band sensors that allow continuous monitoring of, e.g., NDVI. These results suggest that waveband combinations not exploited by presently used (conventional) VIs may offer considerable potential for predicting grassland CO₂ fluxes; this has implications for the design and capabilities of future space, airborne or ground-based low-cost sensors. In particular, these results also have a strong impact on our ability to upscale grassland $f_{\text{APARgreen}}$ and carbon fluxes using future sensors (e.g. Sentinel 2).

The evaluation of the models for the main data set against three new sites showed that at least some of these models can be transferred to predict carbon fluxes and ecophysiological parameters for similar grasslands (Fig. 7). However, for some parameters (e.g. ε), the independent validation indicated a poor performance; it challenges the current practice in upscaling to larger regions by grouping all grasslands into a single plant functional type (PFT). We advocate more studies to be conducted merging CO₂ flux with hyperspectral data by means of models which use a more process-oriented and coupled approach to simulating canopy CO₂ exchange and reflectance in order to explore the causes underlying the observed differences between seemingly closely related study sites.

4.2 Grassland structural characteristics and their spectral response

Although we considered similar ecosystems (belonging to the same vegetation type), the investigated canopies were very different and included Mediterranean, extensive alpine

Table 5. Results of the correlation (R^2 – coefficient of determination) between the best NDS-, SR- and SD-type indices selected for α , GPP_{\max} , midday GPP, midday ε and midday NEE and dry phytomass, nitrogen and water content for Amplero, Neustift, Monte Bondone and all sites pooled. The selected bands for computing NSD-, SR- and SD-type indices are reported in brackets. Statistical significance is indicated as * ($p < 0.05$), ** ($p < 0.01$) and *** ($p < 0.001$).

| Index | Site | Parameter | α R^2 (–) | GPP_{\max} R^2 (–) | GPP R^2 (–) | ε R^2 (–) | NEE R^2 (–) |
|---------------|---------------|-------------------------------|-------------------------------|------------------------------|---------------------|-------------------------------|---------------------|
| NSD-type | Amplero | Dry phytomass ($g\ m^{-2}$) | 0.66** | 0.72** | 0.58* | 0.76** | 0.36 |
| | Amplero | Nitrogen content (%) | 0.30 | 0.32 | 0.19 | 0.49* | 0.15 |
| | Amplero | Water content (%) | 0.28 | 0.53* | 0.56* | 0.44 | 0.55* |
| | Neustift | Dry phytomass ($g\ m^{-2}$) | 0.00 | 0.26 | 0.35 | 0.44* | 0.02 |
| | Neustift | Nitrogen content (%) | 0.16 | 0.15 | 0.21 | 0.77** | 0.03 |
| | Neustift | Water content (%) | 0.00 | 0.00 | 0.03 | 0.59* | 0.10 |
| | Monte Bondone | Dry phytomass ($g\ m^{-2}$) | 0.02 | 0.59*** | 0.49*** | 0.55*** | 0.49*** |
| | Monte Bondone | Nitrogen content (%) | 0.08 | 0.52*** | 0.38** | 0.48*** | 0.38** |
| | Monte Bondone | Water content (%) | 0.09 | 0.48*** | 0.35** | 0.42*** | 0.35** |
| | All | Dry phytomass ($g\ m^{-2}$) | 0.05 | 0.02 | 0.02 | 0.05 | 0.00 |
| | All | Nitrogen content (%) | 0.26*** | 0.04 | 0.02 | 0.41*** | 0.09 |
| | All | Water content (%) | 0.00 | 0.01 | 0.01 | 0.10* | 0.00 |
| | SR-type | Amplero | Dry phytomass ($g\ m^{-2}$) | 0.66** | 0.72** | 0.58* | 0.76* |
| Amplero | | Nitrogen content (%) | 0.30 | 0.32 | 0.20 | 0.49* | 0.15 |
| Amplero | | Water content (%) | 0.28 | 0.53* | 0.56* | 0.44 | 0.55* |
| Neustift | | Dry phytomass ($g\ m^{-2}$) | 0.00 | 0.26 | 0.35 | 0.44* | 0.02 |
| Neustift | | Nitrogen content (%) | 0.16 | 0.15 | 0.21 | 0.77** | 0.03 |
| Neustift | | Water content (%) | 0.01 | 0.00 | 0.03 | 0.59* | 0.10 |
| Monte Bondone | | Dry phytomass ($g\ m^{-2}$) | 0.02 | 0.50*** | 0.50*** | 0.55*** | 0.45* |
| Monte Bondone | | Nitrogen content (%) | 0.08 | 0.48*** | 0.38** | 0.48*** | 0.35 |
| Monte Bondone | | Water content (%) | 0.09 | 0.44*** | 0.34** | 0.41*** | 0.30* |
| All | | Dry phytomass ($g\ m^{-2}$) | 0.08 | 0.01 | 0.01 | 0.05 | 0.00 |
| All | | Nitrogen content (%) | 0.26*** | 0.03 | 0.02 | 0.40*** | 0.09 |
| All | | Water content (%) | 0.00 | 0.01 | 0.01 | 0.11* | 0.00 |
| SD-type | | Amplero | Dry phytomass ($g\ m^{-2}$) | 0.64*** | 0.81** | 0.59* | 0.58* |
| | Amplero | Nitrogen content (%) | 0.22 | 0.30 | 0.22 | 0.30 | 0.03 |
| | Amplero | Water content (%) | 0.16 | 0.45* | 0.59* | 0.19 | 0.49* |
| | Neustift | Dry phytomass ($g\ m^{-2}$) | 0.21 | 0.04 | 0.37 | 0.20 | 0.00 |
| | Neustift | Nitrogen content (%) | 0.11 | 0.01 | 0.12 | 0.81** | 0.08 |
| | Neustift | Water content (%) | 0.02 | 0.26 | 0.00 | 0.64* | 0.52* |
| | Monte Bondone | Dry phytomass ($g\ m^{-2}$) | 0.15 | 0.42*** | 0.36** | 0.45*** | 0.36** |
| | Monte Bondone | Nitrogen content (%) | 0.28*** | 0.34** | 0.34** | 0.38** | 0.35** |
| | Monte Bondone | Water content (%) | 0.27*** | 0.34** | 0.34 | 0.31** | 0.30** |
| | All | Dry phytomass ($g\ m^{-2}$) | 0.20*** | 0.01 | 0.00 | 0.30*** | 0.01 |
| | All | Nitrogen content (%) | 0.01 | 0.01 | 0.02 | 0.02 | 0.11* |
| | All | Water content (%) | 0.01 | 0.03 | 0.04 | 0.28*** | 0.06 |

and intensive alpine grasslands with very different canopy structures in terms of leaf orientation, amount and spatial distribution of green and non-photosynthetic components, leaf nitrogen, and water content, as detailed in Vescovo et al. (2012).

For Amplero and Neustift, NSD-type indices performed well for NIR-vs.-NIR band combinations for all investigated parameters, while Monte Bondone showed best performances in the VIS-vs.-NIR band combinations for GPP_{\max}

and ε (Fig. 6). The dry phytomass was the main driving factor in the spectral response in NIR-vs.-NIR band combinations for Amplero, while nitrogen content drove the spectral response in NIR-vs.-NIR band combinations of Neustift for all parameters except for α (Tables 5 and S6). Interestingly, for Monte Bondone both dry phytomass and nitrogen content explained the spectral response of the grassland in VIS-vs.-NIR band combinations for GPP_{\max} and ε , while no significant relationships with biophysical variables were found for

α , GPP or NEE. These results partially confirm the findings of Vescovo et al. (2012), who highlighted a strong relationship, for several grassland types, between an NSD-type index and phytomass.

For Monte Bondone, NSD- and SR-type indices for the selected bands for estimating all variables except α were strongly correlated with canopy-total chlorophyll content ($R^2 > 0.85$).

The chlorophyll indices (e.g. red-edge NDVI and CI; see Tables 3 and 4) – which are considered the best indices for estimating carbon fluxes in grasslands and crops – showed a good performance for Amplero and Monte Bondone in our data set but performed poorly for Neustift.

It was demonstrated by many authors that the red-edge domain, where reflectance changes from very low in the absorption region to high in the NIR, is one of the best descriptors of chlorophyll concentration. On the other hand, it is well-known that the canopy structure can be a very strong confounding factor. Our results confirm that this topic needs to be further investigated, as this finding has a relevant impact concerning the use of Sentinel 2 to upscale f_{APAR} and carbon flux observations.

It is interesting to see that the NSD-type indices in the NIR-vs.-NIR band combinations appeared to be the best proxy for GPP fluxes when all the grasslands were pooled together. These results can be linked to the controversial paper focused on the strong impact of structure on the ability to estimate canopy nitrogen content (Knyazikhin et al., 2012) and confirm the need for more studies in this direction. Good relationships were found between the NIR-vs.-NIR band combinations (> 750 nm wavelengths) and fluxes; the physical basis of these relationships needs to be further investigated. In fact, it is important to highlight that the literature indicates that the wavelengths in the NIR (> 750 nm) are not sensitive to chlorophyll content, but they are related to leaf, canopy structure and – around the 970 nm area – to water.

As confirmed by comparing the correlation matrix approach with the GA-rF approach, we could not find a universal relationship between reflectance in specific wavelengths of the light spectrum and biophysical properties of vegetation. We think that this is strongly linked to vegetation structure effects. For this reason we believe that further research is necessary to disentangle the impact of factors such as bidirectional reflectance distribution function and scaling effects.

5 Conclusions

The present study focused on understanding the potential of hyperspectral VIs in predicting grassland CO₂ exchange and ecophysiological parameters (α , ε and GPP_{max}) for different European mountain grasslands.

The major finding of this study is that the relationship between ground-based hyperspectral reflectance and the ecosystem-scale CO₂ exchange of mountain grasslands is

much more variable than what might be supposed given this closely related group of structurally and functionally similar ecosystems. As a consequence, the unique models of mountain grassland CO₂ exchange, i.e. the best-fitting models for all sites pooled, explained 47 and 68 % of the variability in the independent variables when established VIs and optimized hyperspectral VIs, respectively, were used. Interestingly, VIs based on reflectance either in the visible or NIR part of the electromagnetic spectrum were superior in predicting mountain grassland CO₂ exchange and ecophysiological parameters compared to commonly used VIs, which are based on a combination of these two wavebands. The band selection based on the GA-rF algorithm confirmed that it is difficult to define a universal band range able to describe ecophysiological parameters, carbon fluxes and biophysical variables, even for a closely related group of ecosystems.

The take-home message from this study thus is that continuing efforts are required to better understand differences in the relationship between ecosystem-scale reflectance and CO₂ exchange and to improve models of this relationship which can be employed to upscale the land-CO₂ exchange to larger spatial scales based on optical remote-sensing data. Initiatives such as SpecNet (<http://specnet.info>; Gamon et al., 2006), the COST Action ES0903 (EUROSPEC; <http://cost-es0903.fem-environment.eu/>) and the COST Action ES1309 (OPTIMISE; http://www.cost.eu/domains_actions/essem/Actions/ES1309) are instrumental in this as they provide the scale-consistent combination of hyperspectral reflectance and CO₂ exchange data.

The Supplement related to this article is available online at doi:10.5194/bg-12-3089-2015-supplement.

Acknowledgements. M. Balzarolo acknowledges the support by the Methusalem program of the Flemish Government. L. Vescovo and D. Gianelle acknowledge the financial support obtained by the EU project CARBOEUROPE-IP (GOCE-CT-2003-505572) and the CARBOITALY project funded by the Italian Government. G. Wohlfahrt and A. Hammerle acknowledge financial support by the Austrian National Science Fund (FWF) through grant agreements P17562 and P26425 and the Tyrolean Science Fund through grant agreement UNI-404/33. A. Hammerle was financially supported by a DOC fellowship from the Austrian Academy of Sciences (ÖAW). E. Tomelleri acknowledges the support of the Province of Bolzano/Bozen through the project MONALISA. Article processing charges of this paper were covered by the EuroSpec COST action (ES0903).

Edited by: M. Rossini



This publication was supported by COST – www.cost.eu

References

- Aubinet, M., Grelle, A., Ibrom, A., Rannik, U., Moncrieff, J., Foken, T., Kowalski, P., Martin, P., Berbigier, P., Bernhofer, C., Clement, R., Elbers, J., Granier, A., Grunwald, T., Morgenster, K., Pilegaard, K., Rebmann, C., Snijders, W., Valentini, R., and Vesala, T.: Estimates of the annual net carbon and water exchange of European forests: the EUROFLUX methodology, *Adv. Ecol. Res.*, 30, 113–75, 2000.
- Aubinet, M., Vesala, T., and Papale, D.: *Eddy Covariance - A Practical Guide to Measurement and Data Analysis*, Springer, ISBN 978-94-007-2351-1, 2012.
- Bacour, C., Baret, F., and Jacquemoud, S.: Information content of HyMap hyperspectral imagery, *Proceedings of the 1st International Symposium on Recent Advances in Quantitative Remote Sensing*, Valencia (Spain), 503–508, 2002a.
- Bacour, C., Jacquemoud, S., Leroy, M., Hauteceur, O., Weiss, M., Prévot, L., Bruguier, L., and Chauki H.: Reliability of the estimation of vegetation characteristics by inversion of three canopy reflectance models on airborne POLDER data, *Agronomie*, 22, 555–565, 2002b.
- Baldocchi, D., Valentini, R., Running, S., Oechel, W., and Dahlman, R.: Strategies for measuring and modelling carbon dioxide and water vapour fluxes over terrestrial ecosystems, *Glob. Change Biol.*, 2, 159–168, 1996.
- Balzarolo, M.: *Biometric parameters and fluxes estimations in Mediterranean mountainous grassland with remote sensing techniques*, PhD thesis, University of Tuscia, 2008.
- Balzarolo, M., Anderson, K., Nichol, C., Rossini, M., Vescovo, L., Arriga, N., Wohlfahrt, G., Calvet, J.-C., Carrara, A., Cerasoli, S., Cogliati, S., Daumard, F., Eklundh, L., Elbers, J. A., Evrendilek, F., Handcock, R. N., Kaduk, J., Klumpp, K., Longdoz, B., Matteucci, G., Meroni, M., Montagnani, L., Ourcival, J.-M., Sanchez-Canete, E. P., Pontailier, J.-Y., Juszczak, R., Scholes, B., and Pilar Martin, M.: Ground-based optical measurements at European flux sites: a review of methods, instruments and current controversies, *Sensors*, 11, 7954–7981, 2011.
- Baret, F., Jacquemoud, S., Guyot, G., and Leprieur, C.: Modeled analysis of the biophysical nature of spectral shifts and comparison with information content of broad bands, *Remote Sens. Environ.*, 41, 133–142, 1992.
- Barnes, J. D., Balaguer, L., Manrique, E., Elvira, S., and Davison, A. W.: A reappraisal of the use of DMSO for the extraction and determination of chlorophylls a and b in lichens and higher plants, *Environ. Exp. Bot.*, 32, 85–100, 1992.
- Beer, C., Reichstein, M., Tomelleri, E., Ciais, P., Jung, M., Carvalhais, N., Rodenbeck, C., Arain, M. A., Baldocchi, D., Bonan, G. B., Bondeau, A., Cescatti, A., Lasslop, G., Lindroth, A., Lomas, M., Luysaert, S., Margolis, H., Oleson, K. W., Rouspard, O., Veenendaal, E., Viovy, N., Williams, C., Woodward, F. I., and Papale, D.: Terrestrial gross carbon dioxide uptake: global distribution and covariation with climate, *Science*, 329, 834–838, 2010.
- Breiman, L.: *Random Forests*, *Mach. Learn.*, 45, 5–32, 2001.
- Cernusca, A., Bahn, M., Berninger, F., Tappeiner, U., and Wohlfahrt, G.: Effects of land-use changes on sources, sinks and fluxes of carbon in European mountain grasslands, *Ecosystems*, 11, 1335–1337, 2008.
- Ciais, P., Wattenbach, M., Vuichard, N., Smith, P., Piao, S. L., Don, A., Luysaert, S., Janssens, I. A., Bondeau, A., Dechow, R., Leip, A., Smith, P. C., Beer, C., van der Werf, G. R., Gervois, S., Van Oost, K., Tomelleri, E., Freibauer, A., Schulze, E. D., and Team, C. S.: The European carbon balance, Part 2: Croplands, *Glob. Change Biol.*, 16, 1409–1428, 2010.
- Clevers, J. G. P. W., Kooistra, L., and Schaepman, M. E.: Estimating canopy water content using hyperspectral remote sensing data, *Int. J. Appl. Earth Observ. Geoinform.*, 12, 119–125, 2010.
- Colombo, R., Meroni, M., Marchesi, A., Busetto, L., Rossini, M., Giardino, C., and Panigada, C.: Estimation of leaf and canopy water content in poplar plantations by means of hyperspectral indices and inverse modeling, *Remote Sens. Environ.*, 112, 1820–1834, 2008.
- Coops, N. C., Hilker, T., Hall, F. G., Nichol, C. J., and Drolet, G. G.: Estimation of light-use efficiency of terrestrial ecosystem from space: a status report, *Bioscience*, 60, 788–797, 2010.
- Drolet, G. G., Huemmrich, K. F., Hall, F. G., Middleton, E. M., Black, T. A., Black, T., Barr, A., Barr, A. A., and Margolis, H.: A MODIS-derived photochemical reflectance index to detect interannual variations in the photosynthetic light-use efficiency of a boreal deciduous forest, *Remote Sens. Environ.*, 98, 212–224, 2005.
- EEA: *Agriculture and environment in EU-15, The IRENA Indicator Report*, EEA, Copenhagen, ISBN 92-9167-779-5, 2005.
- Fava, F., Colombo, R., Bocchi, S., Meroni, M., Sitzia, M., Fois, N., and Zucca, C.: Identification of hyperspectral vegetation indices for Mediterranean pasture characterization, *Int. J. Appl. Earth Obs. Geoinf.*, 11, 233–243, 2009.
- Filella, I., Peñuelas, J., Llorens, L., and Estiarte, M.: Reflectance assessment of seasonal and annual changes in biomass and CO₂ uptake of a Mediterranean shrubland submitted to experimental warming and drought, *Remote Sens. Environ.*, 90, 308–318, 2004.
- Frankenberg, C., Fisher, J. B., Worden, J., Badgley, G., Saatchi, S. S., Lee, J.-E., Toon, G. C., Butz, A., Jung, M., Kuze, A., and Yokota, T.: New global observations of the terrestrial carbon cycle from GOSAT: patterns of plant fluorescence with gross primary productivity, *Geophys. Res. Lett.*, 38, L17706, doi:10.1029/2011gl048738, 2011.
- Gamon, J. A., Peñuelas, J., and Field, C. B.: A narrow-waveband spectral index that tracks diurnal changes in photosynthetic efficiency, *Remote Sens. Environ.*, 41, 35–44, 1992.
- Gamon, J. A., Field, C. B., Fredeen, A. L., and Thayer, S.: Assessing photosynthetic downregulation in sunflower stands with an optically-based model, *Plant Biol.*, 67, 113–125, 2001.
- Gamon, J. A., Rahman, A. F., Dungan, J. L., Schildhauer, M., and Huemmrich, K. F.: Spectral Network (SpecNet): What Is It and Why Do We Need It?, *Remote Sens. Environ.*, 103, 227–235, 2006.
- Gamon, J. A., Coburn, C., Flanagan, L. B., Huemmrich, K. F., Kiddle, C., Sanchez-Azofeifa, G. A., Thayer, D. R., Vescovo, L., Gianelle, D., Sims, D. A., Rahman, A. F., and Pastorello, G. Z.: SpecNet revisited: bridging flux and remote sensing communities, *Can. J. Remote Sens.*, 36, S376–S390, 2010.
- Garbulsky, M. F., Peñuelas, J., Gamon, J., Inoue, Y., and Filella, I.: The photochemical reflectance index (PRI) and the remote sensing of leaf, canopy and ecosystem radiation use efficiencies – a review and meta-analysis, *Remote Sens. Environ.*, 115, 281–297, 2011.

- Gianelle, D., Vescovo, L., Marcolla, B., Manca, G., and Cescatti, A.: Ecosystem carbon fluxes and canopy spectral reflectance of a mountain meadow, *Int. J. Remote Sens.*, 30, 435–449, 2009.
- Gilmanov, T. G., Soussana, J. F., Aires, L., Allard, V., Ammann, C., Balzarolo, M., Barcza, Z., Bernhofer, C., Campbell, C. L., Cernusca, A., Cescatti, A., Clifton-Brown, J., Dirks, B. O. M., Dore, S., Eugster, W., Fuhrer, J., Gimeno, C., Gruenwald, T., Haszpra, L., Hensen, A., Ibrom, A., Jacobs, A. F. G., Jones, M. B., Lanigan, G., Laurila, T., Lohila, A., Manca, G., Marcolla, B., Nagy, Z., Pilegaard, K., Pinter, K., Pio, C., Raschi, A., Rogiers, N., Sanz, M. J., Stefani, P., Sutton, M., Tuba, Z., Valentini, R., Williams, M. L., and Wohlfahrt, G.: Partitioning European grassland net ecosystem CO₂ exchange into gross primary productivity and ecosystem respiration using light response function analysis, *Agr. Ecosyst. Environ.*, 121, 93–120, 2007.
- Gitelson, A. A. and Merzlyak, M. N.: Remote estimation of chlorophyll content in higher plant leaves, *Int. J. Remote Sens.*, 18, 2691–2697, 1994.
- Gitelson, A. A., Viña, A., Ciganda, V., Rundquist, D. C., and Arkebauer, T. J.: Remote estimation of canopy chlorophyll content in crops, *Geophys. Res. Lett.*, 32, L08403, doi:10.1029/2005GL022688, 2005.
- Gitelson, A. A., Viña, A., Rundquist, D. C., Arkebauer, T. J., Keydan, G., Leavitt, B., Ciganda, V., Burba, G. G., and Suyker, A. E.: Relationship between gross primary production and chlorophyll content in crops: Implications for the synoptic monitoring of vegetation productivity, *Geophys. Res. Lett.*, 111, D08S11, doi:10.1029/2005JD006017, 2006.
- Gitelson, A. A., Vina, A., Masek, J. G., Verma, S. B., and Suyker, A. E.: Synoptic monitoring of gross primary productivity of maize using Landsat data, *IEEE Geosci. Remote S.*, 5, 133–137, 2008.
- Gitelson, A. A., Peng, Y., Masek, J. G., Rundquist, D. C., Verma, S., Suyker, A., Baker, J. M., Hatfield, J. L., and Meyers, T.: Remote estimation of crop gross primary production with Landsat data, *Remote Sens. Environ.*, 121, 404–414, 2012.
- Goerner, A., Reichstein, M., Tomelleri, E., Hanan, N., Rambal, S., Papale, D., Dragoni, D., and Schimmlius, C.: Remote sensing of ecosystem light use efficiency with MODIS-based PRI, *Biogeosciences*, 8, 189–202, doi:10.5194/bg-8-189-2011, 2011.
- Grossman, Y. L., Ustin, S. L., Sanderson, E., Jacquemoud, J., Schmuck, G., and Verdebout J.: Critique of stepwise multiple linear regression for the extraction of leaf biochemistry information from leaf reflectance data, *Remote Sens. Environ.*, 56, 182–193, 1996.
- Hmimina, G., Dufrêne, E., and Soudani, K.: Relationship between photochemical reflectance index and leaf ecophysiological and biochemical parameters under two different water statuses: towards a rapid and efficient correction method using real-time measurements, *Plant Cell Environ.*, 37, 473–487, 2014.
- Huete, A. R., Liu, H. Q., Batchily, K., and van Leeuwen, W. J. D.: A comparison of vegetation indices over a global set of TM images for EOS-MODIS, *Remote Sens. Environ.*, 59, 440–451, 1997.
- Inoue, Y., Peñuelas, J., Miyata, A., and Mano, M.: Normalized difference spectral indices for estimating photosynthetic efficiency and capacity at a canopy scale derived from hyperspectral and CO₂ flux measurements in rice, *Remote Sens. Environ.*, 112, 156–172, 2008.
- Jacquemoud, S.: Inversion of the PROSPECT+SAIL canopy reflectance model from AVIRIS equivalent spectra: Theoretical study, *Remote Sens. Environ.*, 44, 281–292, 1993.
- Jacquemoud, S., Bacour, C., Poilvé, H., and Frangi, I.-P.: Comparison of four radiative transfer models to simulate plant canopies reflectance: direct and inverse mode, *Remote Sens. Environ.*, 74, 471–481, 2000.
- Jordan, C. F.: Derivation of leaf area index from quality of light on the forest floor, *Ecology*, 50, 663–666, 1969.
- Kiniry, J. R., Burson, B. L., Evers, G. W., Williams, J. R., Sanchez, H., Wade, C., Featherston, J. W., and Greenwade J.: Coastal bermudagrass, bahiagrass, and native range simulation for diverse sites in Texas, *Agron. J.*, 99, 450–61, 2007.
- Knyazikhin, Y., Schull, M. A., Stenberg, P., Möttus, M., Rautiainen, M., Yang, Y., Marshak, A., Latorre Carmona, P., Kaufmann, R. K., Lewis, P., Disney, M. I., Vanderbilt, V., Davis, A. B., Baret, F., Jacquemoud, S., Lyapustin, A., and Myneni, R. B.: Hyperspectral remote sensing of foliar nitrogen content, *Proc. Natl. Acad. Sci. USA*, 110, 185–192, 2012.
- Lambers, H., Chapin III, F. S., and Pons, T. L.: *Plant physiological ecology*, Springer-Verlag, Berlin, 540, 1998.
- Li, L., Ustin, S. L., and Riano, D.: Retrieval of fresh leaf fuel moisture content using genetic algorithm – partial least squares modeling (GA-PLS), *Geosci. Remote Lett.*, 4, 216–220, 2007.
- Lichtenthaler, H. K.: Chlorophylls and carotenoids: Pigments of photosynthetic biomembranes, *Methods Enzymol.*, 148, 349–382, 1987.
- Marquardt, D. W.: An Algorithm for Least-Squares Estimation of Nonlinear Parameters, *SIAM J. Appl. Math.*, 11, 431–441, 1963.
- Meroni, M., Rossini, M., Guanter, L., Alonso, L., Rascher, U., Colombo, R., and Moreno, J.: Remote sensing of solar induced chlorophyll fluorescence: review of methods and applications, *Remote Sens. Environ.*, 113, 2037–2051, 2009.
- Meroni, M., Barducci, A., Cogliati, S., Castagnoli, F., Rossini, M., Busetto, L., Migliavacca, M., Cremonese, E., Galvagno, M., Colombo, R., and Morra di Cella, U.: The hyperspectral irradiator, a new instrument for long-term and unattended field spectroscopy measurements, *Rev. Sci. Instrum.* 82, 043106, doi:10.1063/1.3574360, 2011.
- Monteith, J. L.: Solar radiation and productivity in tropical ecosystems, *J. Appl. Ecol.*, 9, 747–766, 1972.
- Monteith, J. L. and Moss, C. J.: Climate and the Efficiency of Crop Production in Britain, *Philos. Trans. R. Soc. London B Biol. Sci.*, 281, 277–294, 1977.
- Moore, C. J.: Frequency response corrections for eddy correlation systems, *Bound.-Lay. Meteorol.*, 37, 17–35, 1986.
- Nichol, C. J., Lloyd, J., Shibistova, O., Arneeth, A., Roser, C., Knohl, A., Matsubara, S., and Grace, J.: Remote sensing of photosynthetic-light-use efficiency of a Siberian boreal forest, *Tellus B*, 54, 677–687, 2002.
- Ollinger, S. V., Richardson, A. D., Martin, M. E., Hollinger, D. Y., Frolking, S., Reich, P. B., Plourde, L. C., Katul, G. G., Munger, J. W., Oren, R., Smith, M.-L., Paw U, K. T., Bolstad, P. V., Cook, B. D., Day, M. C., Martin, T. A., Monson, R. K., and Schmid, H. P.: Canopy nitrogen, carbon assimilation, and albedo in temperate and boreal forests: functional relations and potential climate feedbacks, *Proc. Natl. Acad. Sci. USA*, 105, 19336–19341, 2008.
- Peng, Y., Gitelson, A. A., Keydan, G., Rundquist, D. C., and Moses, W.: Remote estimation of gross primary production in maize and

- support for a new paradigm based on total crop chlorophyll content, *Remote Sens. Environ.*, 115, 978–989, 2011.
- Peñuelas, J. and Filella, I.: Visible and near-infrared reflectance techniques for diagnosing plant physiological status, *Trends Plant Sci.*, 3, 151–156, 1998.
- Peñuelas, J., Filella, I., Biel, C., Serrano, L., and Save, R.: The reflectance at the 950–970 nm region as an indicator of plant water status, *Int. J. Remote Sens.*, 14, 1887–1905, 1993.
- Peñuelas, J., Gamon, J. A., Fredeen, A., Merino, J., and Field, C. B.: Reflectance indices associated with physiological changes in nitrogen- and water-limited sunflower leaves, *Remote Sens. Environ.*, 48, 135–146, 1994.
- Peñuelas, J., Filella, I., and Gamon, J. A.: Assessment of photosynthetic radiation-use efficiency with spectral reflectance, *New Phytol.*, 131, 291–296, 1995.
- Peñuelas, J., Garbulsky, M. F., and Filella, I.: Photochemical reflectance index (PRI) and remote sensing of plant CO₂ uptake, *New Phytol.*, 191, 596–599, 2011.
- Polley, H. W., Phillips, B. L., Frank, A. B., Bradford, J. A., Sims, P. L., Morgan, J. A., and Kiniry, J. R.: Variability in light-use efficiency for gross primary productivity on Great Plains grasslands, *Ecosystems*, 14, 15–27, 2011.
- Rahimzadeh-Bajgirani, P., Munehiro, M., and Omasa, K.: Relationships between the photochemical reflectance index (PRI) and chlorophyll fluorescence parameters and plant pigment indices at different leaf growth stages, *Photosynth. Res.*, 113, 261–271, 2012.
- Riaño, D., Ustin, S. L., Usero, L., and Patricio, M. A.: Estimation of fuel moisture content using neural networks, *Lect. Notes in Comput. Sc.*, 3562, 489–498, 2005a.
- Rossini, M., Meroni, M., Migliavacca, M., Manca, G., Cogliati, S., Busetto, L., Picchi, V., Cescatti, A., Seufert, G., and Colombo, R.: High resolution field spectroscopy measurements for estimating gross ecosystem production in a rice field, *Agr. Forest Meteorol.*, 150, 1283–1296, 2010.
- Rossini, M., Cogliati, S., Meroni, M., Migliavacca, M., Galvagno, M., Busetto, L., Cremonese, E., Julitta, T., Siniscalco, C., Morra di Cella, U., and Colombo, R.: Remote sensing-based estimation of gross primary production in a subalpine grassland, *Biogeosciences*, 9, 2565–2584, doi:10.5194/bg-9-2565-2012, 2012.
- Rouse, J. W., Haas, R. H., Schell, J. A., and Deering, D. W.: Monitoring vegetation systems in the Great Plains with ERTS, 3rd ERTS Symposium, NASA SP-351 I, 1973.
- Sakowska, K., Vescovo, L., Marcolla, B., Juszczak, R., Olejnik, J., and Gianelle, D.: Monitoring of carbon dioxide fluxes in a subalpine grassland ecosystem of the Italian Alps using a multispectral sensor, *Biogeosciences*, 11, 4695–4712, doi:10.5194/bg-11-4695-2014, 2014.
- Schwalm, C. R., Black, T. A., Arniro, B. D., Arain, M. A., Barr, A. G., Bourque, C. P. A., Dunn, A. L., Flanagan, L. B., Giason, M.-A., Lafleur, P. M., Margolis, H. A., McCaughey, J. H., Orchansky, A. L., and Wofsy, S. C.: Photosynthetic light use efficiency of three biomes across an East–west continental-scale transect in Canada, *Agr. Forest Meteorol.*, 140, 269–286, 2006.
- Sims, D. A. and Gamon, J. A.: Relationships between leaf pigment content and spectral reflectance across a wide range of species, leaf structures, and developmental stages, *Remote Sens. Environ.*, 81, 337–354, 2002.
- Soudani, K., Hmimina, G., Dufrêne, E., Berveiller, D., Delpierre, N., Ourcival, J.-M., Rambal, S., and Joffre, R.: Relationships between photochemical reflectance index and light-use efficiency in deciduous and evergreen broadleaf forests, *Remote Sens. Environ.*, 144, 73–84, 2014.
- Soussana, J. F., Allard, V., Pilegaard, K., Ambus, C., Campbell, C., Ceschia, E., Clifton-Brown, J., Czobel, S., Domingues, R., Flechard, C., Fuhrer, J., Hensen, A., Horvath, L., Jones, M., Kasper, G., Martin, C., Nagy, Z., Neftel, A., Raschi, A., Baronti, S., Rees, R. M., Skiba, U., Stefani, P., Manca, G., Sutton, M., Tuba, Z., and Valentini, R.: Full accounting of the greenhouse gas (CO₂, N₂O, CH₄) budget of nine European grassland sites, *Agri. Eco. Environ.*, 121, 121–134, 2007.
- Vescovo L., Wohlfahrt, G., Balzarolo, M., Pilloni, S., Sottocornola, M., Rodeghiero, M., and Gianelle, D.: New spectral vegetation indices based on the near-infrared shoulder wavelengths for remote sensing detection of grassland phytomass, *Int. J. Remote Sens.*, 33, 2178–2195, 2012.
- Waring, R. and Running, S. W.: *Forest Ecosystems: Analysis at Multiple Scales*, Elsevier, New York, 1998.
- Webb, E. K., Pearman, G. I., and Leuning, R.: Correction of flux measurements for density effects due to heat and water vapour transfer, *Q. J. Roy. Meteorol. Soc.*, 106, 85–100, 1980.
- Wilczak, J. M., Oncley, S. P., and Stage, S. A.: Sonic anemometer tilt correction algorithms, *Bound.-Lay. Meteorol.*, 99, 127–150, 2001.
- Wohlfahrt, G., Sapinsky, S., Tappeiner, U., and Cernusca, A.: Estimation of plant area index of grasslands from measurements of canopy radiation profiles, *Agr. Forest Meteorol.*, 109, 1–12, 2001.
- Wohlfahrt, G., Anderson-Dunn, M., Bahn, M., Balzarolo, M., Berninger, F., Campbell, C., Carrara, A., Cescatti, A., Christensen, T., Dore, S., Eugster, W., Friborg, T., Furger, M., Gianelle, D., Gimeno, C., Hargreaves, K., Hari, P., Haslwanter, A., Johansson, T., Marcolla, B., Milford, C., Nagy, Z., Nemitz, E., Rogiers, N., Sanz, M.J., Siegwolf, R. T. W., Susiluoto, S., Sutton, M., Tuba, Z., Ugolini, F., Valentini, R., Zorer, R., and Cernusca, A.: Biotic, abiotic and management controls on the net ecosystem CO₂ exchange of European mountain grasslands, *Ecosystems*, 11, 1338–1351, 2008.
- Wohlfahrt, G., Pilloni, S., Hörtnagl, L., and Hammerle, A.: Estimating carbon dioxide fluxes from temperate mountain grasslands using broad-band vegetation indices, *Biogeosciences*, 7, 683–694, doi:10.5194/bg-7-683-2010, 2010.
- Zarco-Tejada, P. J., Rueda, C. A., and Ustin, S. L.: Water content estimation in vegetation with MODIS reflectance data and model inversion method, *Remote Sens. Environ.*, 85, 109–124, 2003.